

Review

Recent Advances in Electrocatalytic Oxidation of 5-Hydroxymethylfurfural to 2,5-Furandicarboxylic Acid by Heterogeneous Catalysts

Zhiming Ma ^{1,*}, Lei Wang ², Guangyu Li ¹ and Tao Song ^{3,4,5,6,*} 

¹ School of Environmental and Chemical Engineering, Shenyang Ligong University, Shenyang 110159, China; lgych@163.net

² Department of Chemistry and Chemical Engineering, Shenyang Institute of Science and Technology, Shenyang 110167, China; lwang1014@163.com

³ CAS Key Laboratory of Bio-Based Materials, Qingdao Institute of Bioenergy and Bioprocess Technology, Chinese Academy of Sciences, No. 189 Songling Road, Qingdao 266101, China

⁴ University of Chinese Academy of Sciences, Beijing 100049, China

⁵ Shandong Energy Institute, Qingdao 266101, China

⁶ Qingdao New Energy Shandong Laboratory, Qingdao 266101, China

* Correspondence: mazhiming@sylu.edu.cn (Z.M.); songtao@qibebt.ac.cn (T.S.)

Abstract: The utilization and development of biomass resources is an efficient solution to mitigate the fossil energy crisis. Based on the advantages of mild reaction conditions, rapid reaction, and high conversion, the synthesis of 2,5-furandicarboxylic acid (FDCA) by the electrocatalytic oxidation of 5-hydroxymethylfurfural (HMFOR) has attracted considerable attention. This review will summarize the recent advances of HMFOR to FDCA, including the reaction pathway and mechanism, as well as the catalytic performance of various heterogeneous electrocatalysts. The challenges and prospects for HMFOR are also focused on. Finally, it is expected that this work may provide guidance for the design of high-efficiency electrocatalysts and thereby accelerate the industrialization process of biomass utilization.

Keywords: biomass; HMF; HMFOR; FDCA; heterogeneous catalyst



Citation: Ma, Z.; Wang, L.; Li, G.; Song, T. Recent Advances in Electrocatalytic Oxidation of 5-Hydroxymethylfurfural to 2,5-Furandicarboxylic Acid by Heterogeneous Catalysts. *Catalysts* **2024**, *14*, 157.

<https://doi.org/10.3390/catal14020157>

Academic Editor: Simona M. Coman

Received: 19 January 2024

Revised: 15 February 2024

Accepted: 16 February 2024

Published: 19 February 2024



Copyright: © 2024 by the authors. Licensee MDPI, Basel, Switzerland. This article is an open access article distributed under the terms and conditions of the Creative Commons Attribution (CC BY) license (<https://creativecommons.org/licenses/by/4.0/>).

1. Introduction

With the rapid global economic growth, there is an ever-increasing demand for fossil fuels, such as coal, crude oil, and natural gas. However, this has also led to energy crises and environmental issues [1–3]. In 2015, the United Nations set the Sustainable Development Goals (SDGs) to be achieved by 2030. The development of affordable clean energy was recognized as one of the key issues of global concerns. Therefore, it is essential to develop renewable resources and construct sustainable energy systems to alleviate the scarcity of traditional fossil fuels [4]. Lignocellulosic biomass is considered to be the most abundant renewable carbon resource on earth, holding immense potential in achieving carbon-peak and carbon-neutral goals. As a result, it has garnered extensive attention from the scientific community over the past decade [5,6].

5-hydroxymethylfurfural (HMF) is a dehydration product of C₆ carbohydrates derived from biomass. The HMF molecule comprises a furan ring, an aldehyde group, and a hydroxymethyl group, and possess relatively active chemical properties [5]. It can be converted into high-value products and more stable platform molecules through oxidation, reduction, hydrolysis, and esterification reactions. Therefore, HMF is also widely regarded as the “sleeping giant” in the sustainable biorefinery [7,8]. Valuable chemicals derived from the oxidation of HMF include 2,5-diformylfuran (DFF), 5-hydroxymethyl-2-furancarboxylic acid (HMFCA), 5-formyl-2-furancarboxylic acid (FFCA), and 2,5-furandicarboxylic acid (FDCA) [3,9]. Among them, FDCA is recognized as one of the “TOP 10 + 4” most promising

bio-based platform chemicals for establishing a future “green” chemical industry by the U.S. Department of Energy in 2004 [3]. Due to the similarity in structure and chemical properties between FDCA and the traditional petroleum-based monomer terephthalic acid (TPA), which is used to synthesize polyethylene terephthalate (PET), FDCA is expected to replace TPA in the production of bioplastic polyethylene 2,5-furandicarboxylate (PEF). PEF could soon replace PET in the future thanks to its excellent barrier properties, extended mechanical properties, and recyclability [5,7,10]. At present, FDCA has realized commercial production, and the representative enterprises include Avantium and Synbias. Avantium, a Dutch Company, is proposing to construct a new commercial plant for the large-scale industrial production of PEF from FDCA, which will be the world’s first flagship facility for the preparation of FDCA. This facility, located in Delfzijl, Netherlands, is expected to commence operations in 2024 with an annual production capacity of 5000 tons/year of FDCA by utilizing Avantium’s YXY patent technology, which utilizes fructose as a raw material [9]. In addition, FDCA has a wide range of applications, including (1) as monomers for the synthesis of polyesters, polyurethanes, and polyamides; (2) as a precursor for plasticizers; (3) in the synthesis of novel semi-aromatic nylons/semi-bio-based aramids and polyether; (4) in the production of unsaturated resins; and (5) in the fields of thermosetting plastics and coatings [2–4,7,10].

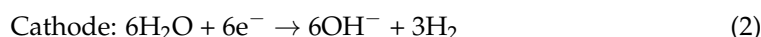
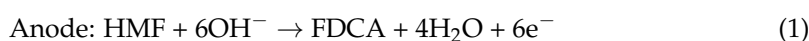
In the early stages, the research on the oxidation of HMF to produce FDCA mainly focused on thermal catalysis. Although it achieved good performance, there were often drawbacks such as high energy input (e.g., requiring high temperatures above 100 °C and high pressures of 10 bar O₂), the use of expensive noble metals (Au, Pt, Ru, and Pd), long reaction times (typically exceeding 10 h), and environmental pollution (involving organic solvents and oxidants) [4,5,11,12]. These disadvantages were against the concept of green production and hindered its large-scale industrial application. In recent years, environmentally friendly and low-energy-consuming methods such as biocatalysis, photocatalysis, and electrocatalysis have garnered widespread attention in the scientific community for the oxidation of HMF to synthesize FDCA [5]. However, biocatalysis and photocatalysis for the conversion of HMF to FDCA is still in the initial stages. Currently, biocatalysis faces challenges in terms of long preparation cycles and the inhibition of reaction intermediates, while photocatalysis suffers from high instrument costs and low energy conversion rates [9]. Recently, electrocatalysis has been extensively studied for the oxidation of HMF to prepare FDCA. This is primarily due to the following advantages: (1) Water is used as the oxygen source, replacing costly pressurized oxidizing gases, thereby ensuring safety and energy efficiency. (2) Lower reaction temperatures and pressures (typically at room temperature) and relatively shorter reaction durations. (3) It can replace noble metal catalysts, as numerous non-noble metal catalysts exhibit excellent performance under alkaline conditions. (4) The reaction rate and oxidation selectivity can be precisely controlled by adjusting electrochemical parameters such as current, potential, electrolyte, and electrocatalyst performance. (5) Value-added chemical products can be obtained on both sides of the electrochemical reactor (i.e., cathode and anode), enhancing the overall system efficiency [4,5].

This review will summarize the latest research progress in the electrocatalytic oxidation of HMF for the synthesis of FDCA. By incorporating the HMFOR reaction pathway and mechanism, a systematic organization and summary of heterogeneous electrocatalysts used for HMFOR have been conducted. The heterogeneous electrocatalysts are classified into two categories depending on whether they contain noble metals in their main constituent materials: noble metal catalysts and non-noble metal catalysts. Emphasis is placed on highlighting the research advancements of non-noble metal catalysts. The further classification of non-noble metal catalysts includes four types: (1) non-noble metal phosphides, sulfides, borides, and nitrides; (2) non-noble metal hydroxides and oxides; (3) heterostructures; (4) and other catalysts such as MOFs, COFs, and non-metal catalysts. Additionally, a summary and outlook of the current research issues and future research directions have been supplied. This is intended to offer guidance and references for the development of efficient and stable electrocatalysts, as well as providing a theoretical

basis and technological support for the high-efficiency catalytic synthesis and large-scale production of FDCA.

2. Reaction Pathway and Mechanism of HMFOR

HMF is a highly functionalized biomass platform molecule, which contains a furan ring, a hydroxymethyl group and an aldehyde group. The process of HMFOR usually follows a three-step reaction involving six electron transfers [2,3]. Generally, it occurs in an alkaline environment in most cases. The electrode reaction formulas are as follows:



2.1. Reaction Pathway

According to the oxidation order of hydroxymethyl and aldehyde groups in HMF, HMFOR can generally be classified into two pathways (Figure 1). In general, the oxidation path of HMF is strongly dependent on the pH value of the electrolyte. HMFOR tends to follow path 1 in a non-strong alkaline environment ($\text{pH} < 13$), while path 2 occurs in a strong alkaline environment ($\text{pH} \geq 13$) [4,5].

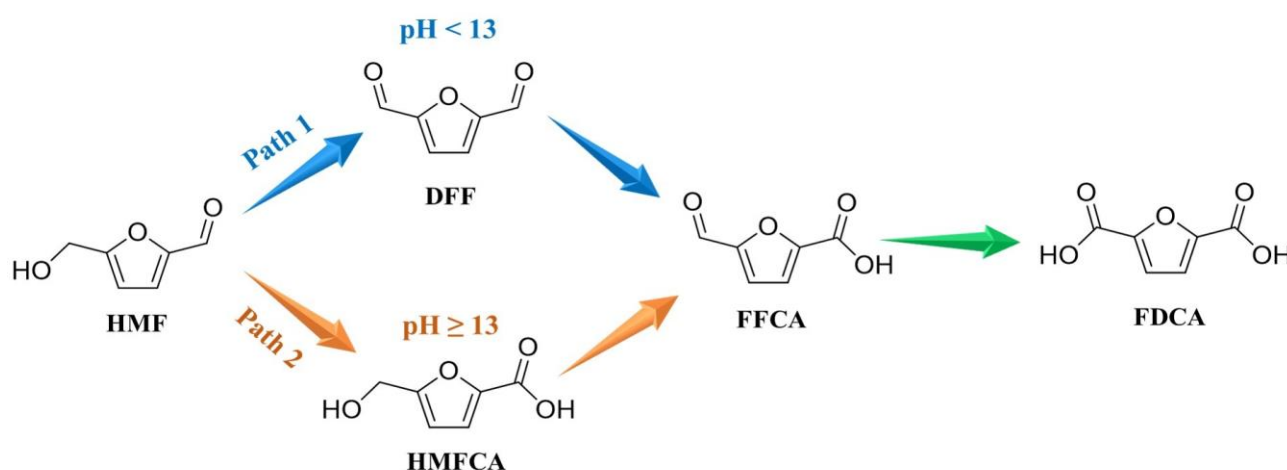


Figure 1. Two reaction pathways of HMFOR.

Linear sweep voltammetry (LSV) is usually used to detect the electrocatalytic activity, chronoamperometry is used to monitor the electrochemical performance of the catalyst, and HPLC is used to analyze the electrolyte [3]. The HMF conversion, FDCA yield, and Faradaic efficiency (FE) of the products are usually calculated using the following equations.

$$\text{Conversion (\%)} = \frac{\text{mol of HMF consumed}}{\text{mol of initial HMF}} \times 100 \quad (4)$$

$$\text{Yield (\%)} = \frac{\text{mol of FDCA formed}}{\text{mol of initial HMF}} \times 100 \quad (5)$$

$$\text{FE (\%)} = \frac{\text{mol of FDCA formed}}{\text{total charge passed}/(F \times 6)} \times 100 \quad (6)$$

where F is the Faraday constant ($96,485 \text{ C mol}^{-1}$).

2.2. Reaction Mechanism

In fact, HMFOR can be classified as a “nucleophilic oxidation reaction” (NOR), which is similar to the oxidation reaction of small organic molecules such as alcohols, aldehydes,

amines, urea, and so on. All of them use nucleophilic groups with active hydrogen (such as hydroxyl, aldehyde, and amino) as the oxidation reaction sites [13–15]. HMFOR can be classified into direct oxidation and indirect oxidation according to whether it needs external voltage to drive substrate oxidation [2,7,10].

2.2.1. Direct Oxidation

Direct oxidation refers to the use of an applied potential to directly drive substrate oxidation, without changing the valence state of the catalyst throughout the entire reaction process [2]. The applied potential promotes the adsorption of OH^- on the electrode, electron transfer, and subsequent substrate dehydrogenation. Specifically, the aldehyde hydration process of HMF is inhibited in a non-strong alkaline environment ($\text{pH} < 13$), while hydroxymethyl is preferentially adsorbed on the electrode surface, triggering the deprotonation of C-H and O-H bonds through the activation of OH^- , thereby producing DFF intermediates. Then, the aldehyde group undergoes a nucleophilic addition reaction with water to generate a geminal diol. The C-H and O-H bonds of the geminal diol are subsequently activated by OH^- and deprotonated to form FFCA. Afterwards, the two steps of nucleophilic addition and deprotonation are repeated to generate FDCA (as seen in Figure 2a). In a strong alkaline environment ($\text{pH} \geq 13$), aldehyde groups will preferentially adsorb on the catalyst surface, react with H_2O to form a geminal diol during alkaline catalysis, and then undergo dehydrogenation to form HMFCFA intermediates by OH^- activation. Subsequently, hydroxymethyl deprotonation generates FFCA. Finally, the two steps of nucleophilic addition and dehydrogenation are repeated to generate FDCA (as seen in Figure 2b) [4,7,10].

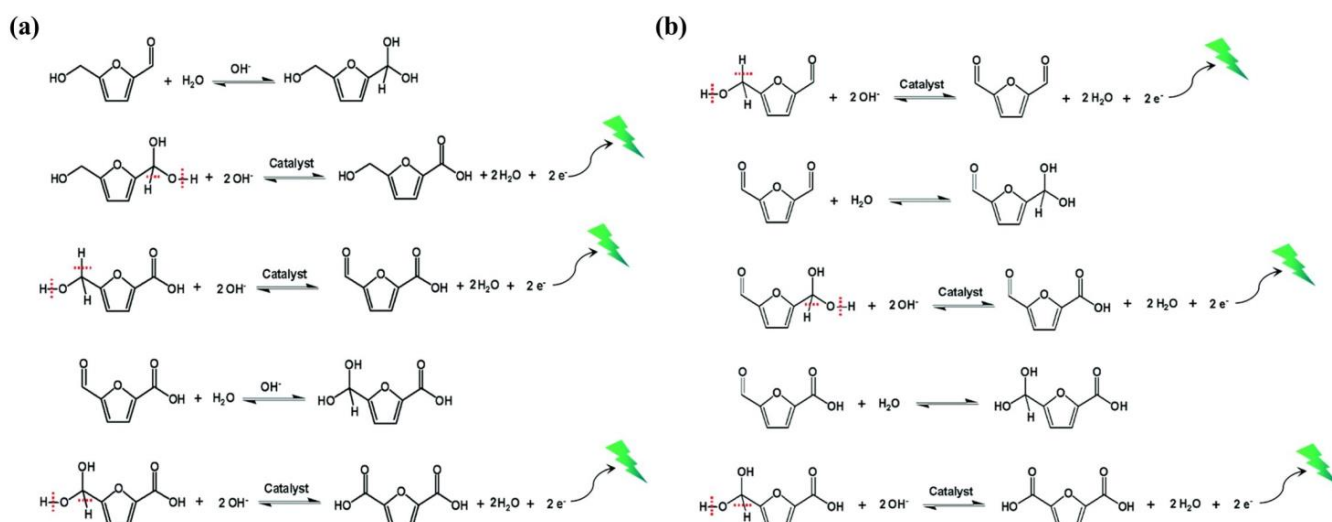


Figure 2. (a) Reaction mechanism of direct oxidation in a strong alkaline environment ($\text{pH} \geq 13$). The applied bias is to promote the adsorption of OH^- on the electrode and rapidly remove electrons deposited onto the surface of the electrode. (b) Reaction mechanism of direct oxidation in a non-strong alkaline environment ($\text{pH} < 13$). The applied bias is to promote the adsorption of OH^- on the electrode and rapidly remove electrons deposited onto the surface of the electrode. Reproduced from Ref. [2]. Copyright 2021, with permission from Royal Society of Chemistry.

2.2.2. Indirect Oxidation

Contrary to direct oxidation, indirect oxidation refers to the catalyst acting as an oxidation–reduction medium to drive substrate oxidation, while the applied potential is only used for the regeneration of the catalyst medium [2,7]. As seen in Figure 3, indirect oxidation typically involves two consecutive processes. Firstly, the medium is electrochemically oxidized from a low-valence/reduced state to a high-valence/oxidized active intermediate (Process 1: $\text{M}^{n+} \rightarrow \text{M}^{n+1}$ ($\text{MOOH}/(\text{MOH})\text{O}$)). Subsequently, the generated high-valence active intermediate (M^{n+1}) will undergo the non-electrochemical oxida-

tion (activation and cleavage of C-H/O-H bonds) of the nucleophilic reagent/substrate through hydride or hydrogen atom transfer (HMF self-dehydrogenation) of the nucleophilic reagent/substrate, as well as M^{n+1} being further reduced to the initial valence state (M^{n+}) (Process 2: $M^{n+1} \rightarrow M^{n+}$) [2,10]. The catalytic medium referred to here can either be a heterogeneous catalyst or a homogeneous catalyst. The difference is that the heterogeneous electrocatalytic oxidation of HMF typically requires the participation of OH^- in the reaction process, while homogeneous catalytic oxidation only requires electron transfer and does not require the participation of OH^- . Therefore, a strongly alkaline environment ($\text{pH} \geq 13$) is more favorable for the heterogeneous catalytic oxidation of HMF [2,7]. In addition, experiments and density functional theory (DFT) calculations have demonstrated that the active sites of the catalyst in this HMF oxidation mechanism are electron-deficient lattice oxygen and adsorbed oxygen, rather than metal sites [4]. Meanwhile, when designing catalysts, it should also be noted that the conversion of M^{n+1} depends on the electrochemical potential, while the subsequent oxidation of HMF depends on the number of active sites or their intrinsic activity [5].

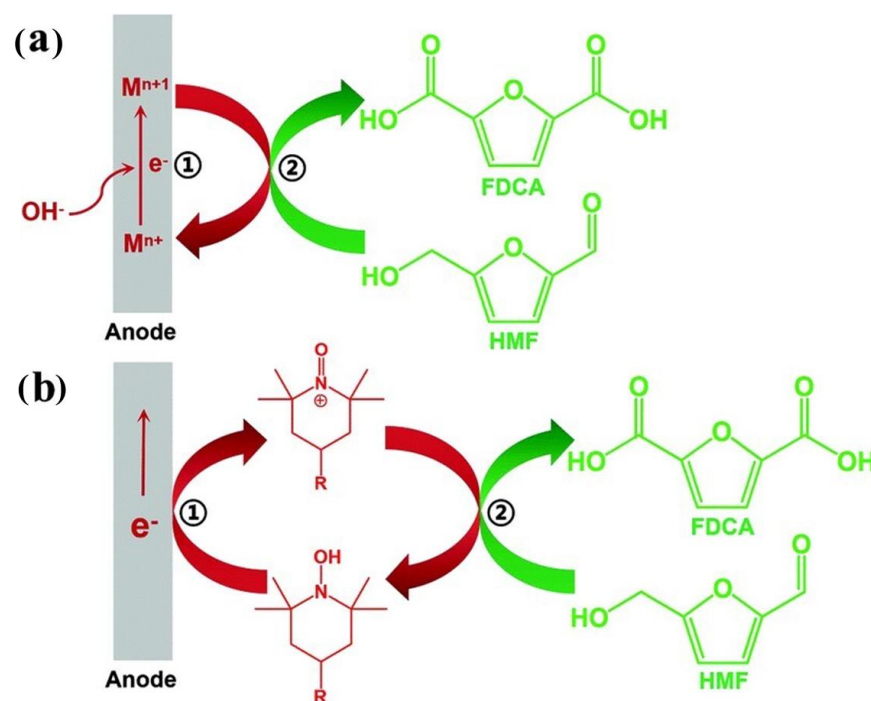


Figure 3. Schematic reaction mechanism of indirect oxidation mediated by (a) a heterogeneous redox mediator (M^{n+} represents low-valence state of the mediator, and M^{n+1} represents high-valence state of the mediator) and (b) a homogeneous redox mediator (taking TEMPO-mediated oxidation as an example). Reproduced from Ref. [2]. Copyright 2021, with permission from Royal Society of Chemistry.

3. Heterogeneous Catalysts for HMFOR to FDCA

In this review, we classify heterogeneous electrocatalysts based on their main components and summarize the research progress of similar catalysts. Specifically, we divide heterogeneous catalysts into two categories: noble metal catalysts and non-noble metal catalysts, depending on whether the materials contain noble metals. Among them, non-noble metal catalysts can be further divided into four types: (1) non-noble metal phosphides, sulfides, borides, and nitrides; (2) non-noble metal hydroxides and oxides; (3) heterostructures; and (4) other catalysts, such as MOFs, COFs, and non-metal catalysts.

3.1. Noble Metal Catalysts

Due to the unique electronic structure and orbital properties of noble metal catalysts, early studies on HMFOR mainly focused on noble metal catalysts [16–19]. Although noble

metal electrocatalysts exhibit low oxidation potentials in HMF, they typically provide very low current densities, which renders them unsuitable as ideal catalysts for HMFOR. Moreover, achieving the complete oxidation of HMF to FDCA using a single noble metal catalyst is challenging [2]. Table 1 summarizes recent advances in the electrocatalytic oxidation of HMF to synthesize FDCA using noble metal catalysts. Pt was the first noble metal used for HMFOR. In 2012, Strasser and co-workers employed Pt/C as an electrode for the electro-oxidation of HMF (Table 1, entry 1) [16]. However, they only achieved a low current density of 0.44 mA cm² and almost negligible production of the target product, FDCA (yield < 1%). In 2019, Ma and co-workers prepared ruthenium(III) polyethyleneimine (Ru(III)-PEI) catalysts supported on carboxyl-modified carbon nanotubes (Ru(III)-PEI@MWCNTs), which showed improved Faradaic efficiency (FE) of up to 94% in an alkaline environment with a pH of 13, and could stably produce FDCA (Table 1, entry 2) [18]. Li and co-workers compared the effects of Au/C and Pd/C catalysts on HMFOR and revealed that the electrode potential and catalyst materials could significantly influence the reaction pathway (Table 1, entries 3–4) [17]. On the Au/C catalyst, aldehyde oxidation is favored over hydroxymethyl oxidation, but the yield of FDCA is negligible (1%). On the other hand, the oxidation pathway of HMF on Pd/C catalyst strongly depends on the applied potential. At low potentials, the DFF pathway is dominant with an FDCA yield of 29%.

Table 1. HMFOR over noble metal catalysts ^a.

Entry	Catalyst	HMF (mM)	Potential (V vs. RHE)	HMF Conversion (%)	FDCA Yield (%)	FE (%)	Ref.
1 ^b	Pt/C	5	-	29	<1	-	[16]
2 ^c	Ru(III)-PEI@MWCNTs	1	1.34	-	-	94	[18]
3 ^c	Au/C	20	0.9	100	1	-	[17]
4 ^c	Pd/C	20	0.9	97	29	-	[17]
5 ^c	Pd ₂ Au ₁ /C	20	0.9	100	64	-	[17]
6 ^c	Pd ₁ Au ₂ /C	20	0.9	100	83	-	[17]
7	(AuPd) ₇	5	0.82	49.3	11.1	72.8	[19]
8	Au ₇ /Pd ₇	5	0.82	33	6.8	83.8	[19]
9	Pd ₇ /Au ₇	5	0.82	42.4	10.1	85.8	[19]
10	Pd-NiCo	50	1.38	99.6	96.5	95.9	[20]
11	Ir-Co ₃ O ₄	50	1.42	-	98	98	[21]
12	Ru ₁ /CoO _x	5	1.45	-	55	55.2	[22]
13	Rh-SA/NiFe NMLDH	50	1.30	98	99.8	98.5	[23]
14	Ru _{0.3} /NiFe	5	1.48	99.43	98.68	-	[24]

^a The electrocatalytic oxidation of HMF was tested in 1.0 M KOH. ^b 0.1 mM NaOH. ^c 0.1 M KOH.

In summary, the conversion of HMF and the yield or selectivity of FDCA were unsatisfactory using a single noble metal as a catalyst [2,3]. Additionally, the high cost and poor catalytic performance of noble metals pose challenges for their industrial-scale production. One approach to overcome these limitations is to construct alloy structures that precisely tune the electronic or geometric properties of the metals. This reduces catalyst preparation costs and improves electrocatalytic oxidation performance [7]. This strategy is advantageous for electron transfer and can modify catalytic activity and selectivity by influencing adsorption, desorption, and surface reactions. The construction of alloy structures takes advantage of the distinctive properties of the alloy components, thereby compensating for the limitations of single metal catalysts and enabling the electrochemical oxidation of HMF for the production of FDCA [4].

Li and co-workers discovered that AuPd bimetallic catalysts exhibited a synergistic effect during HMFOR [17]. The addition of Au to the Pd surface facilitated the oxidation of aldehyde groups at lower potentials and enhanced the hydroxymethyl oxidation activity. As a result, higher yields of FDCA were obtained due to the altered surface composition

and morphology (Table 1, entries 5–6). In 2020, Kim and co-workers developed a 3D hybrid AuPd bimetallic electrode through the layered assembly (LbL) method for HMFOR (Figure 4) [19]. The results revealed that HMFOR was more favorable when the (AuPd)₇ electrocatalyst structure had an alternating arrangement of Au and Pd; the HMF conversion was 49.3% and the FDCA yield was 10.1% (Table 1, entries 7–9).

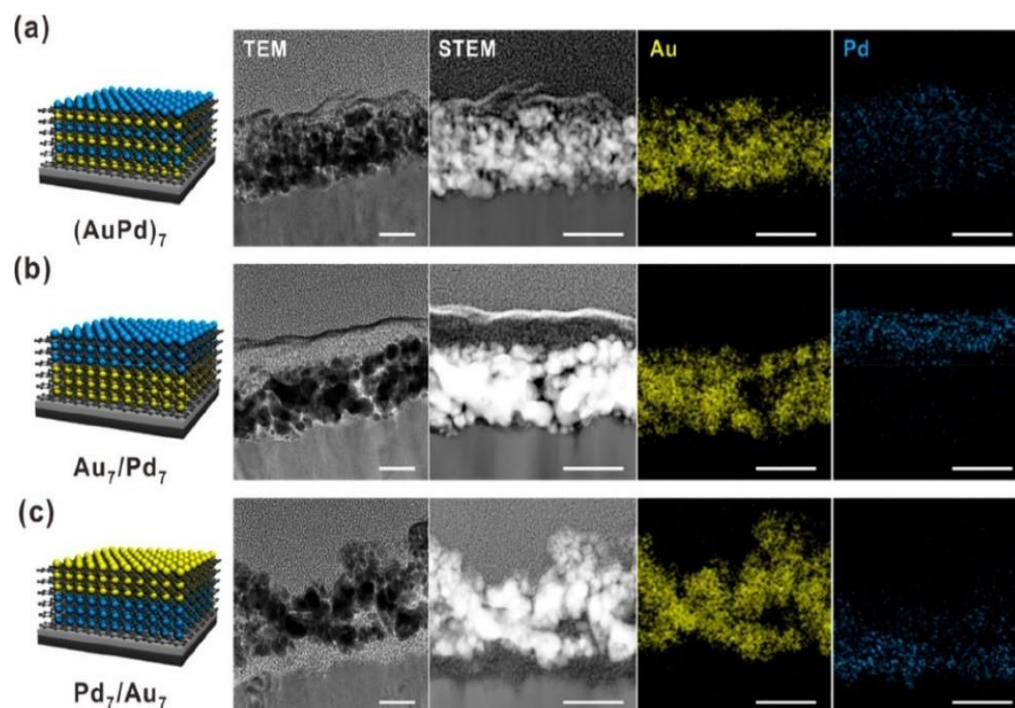


Figure 4. Architecture-controlled multilayer thin-film electrodes. Representative cross-sectional TEM, scanning TEM (STEM), and EDS mapping images of (a) (AuPd)₇, (b) Au₇/Pd₇, and (c) Pd₇/Au₇ multilayer thin-film electrodes assembled on an ITO-coated substrate (scale bar: 50 nm). Reproduced from Ref. [19]. Copyright 2020, with permission from American Chemical Society.

Recently, Song and co-workers prepared Pd/NiCo catalysts by modifying Pd clusters on Co-doped Ni(OH)₂ [20]. It was found that Co doping and Pd loading optimized the catalytic activity of Ni(OH)₂ for HMFOR from thermodynamic and kinetic perspectives, respectively. The introduction of Co caused lattice distortion and optimized the band structure of Ni sites. Pd clusters with an average size of 1.96 nm exhibited electron interactions with NiCo carriers, leading to electron transfer from Pd to Ni sites. This reduced electron transfer impedance and improved the generation rate of Ni³⁺-O. In addition, Pd species further optimized the adsorption of HMF through orbital hybridization, thereby increasing the probability of contact between the Ni³⁺-O active substance and HMF. Pd/NiCo achieved a current density of 50 mA cm⁻² at 1.38 V, HMF conversion of 99.6%, FDCA yield of 96.5%, and an FE of 95.9%, which is superior to most reported catalysts (Table 1, entry 10).

Single-atom catalysts have been widely applied in various catalytic reactions due to their unique metal–support interface induced by their unsaturated coordination environment and maximum atomic utilization efficiency [25–30]. Designing HMFOR single-atom catalysts with active metal loading interfaces may be an effective way to investigate the relationship between catalyst structure and catalytic performance. In 2021, Wang and co-workers employed DFT theoretical calculation and found the weak adsorption capacity of HMF on Co₃O₄, which led to limited reaction activity. After incorporating single-atom Ir sites, the Ir-Co₃O₄ electrocatalyst exhibited stronger adsorption capacity for the C=C group of HMF [21]. This resulted in a heightened adsorption capacity for HMF molecules on Co₃O₄, leading to a reduction in the reaction adsorption energy barrier and a boost in the

reaction kinetics rate. The yield of FDCA was 98%, and the FE was 98% (Table 1, entry 11). This study offers a novel method for the development of efficient electrocatalysts for HMFOR. Recently, Chen and co-workers prepared Ru_1/CoO_x catalysts by impregnating single Ru atoms onto cobalt oxide substrates, which exhibited excellent performance for HMFOR (Table 1, entry 12) [22]. The results indicated that introducing single Ru atoms at an ultra-low load of ~ 0.5 wt.% could accelerate the electroreduction of $\text{Co}^{2+}/\text{Co}^{3+}/\text{Co}^{4+}$, improve the intrinsic activity of CoO_x substrates, and achieve an FDCA selectivity of 76.5%, which is better than the original CoO_x electrocatalyst (62.7%). The interface synergistic effect at the Ru_1/CoO_x interface indicated that single Ru atoms could enhance the adsorption of HMF at the Ru_1/CoO_x interface, thus accelerating the rate-determining step of selective C-H bond activation for FDCA production (Figure 5).

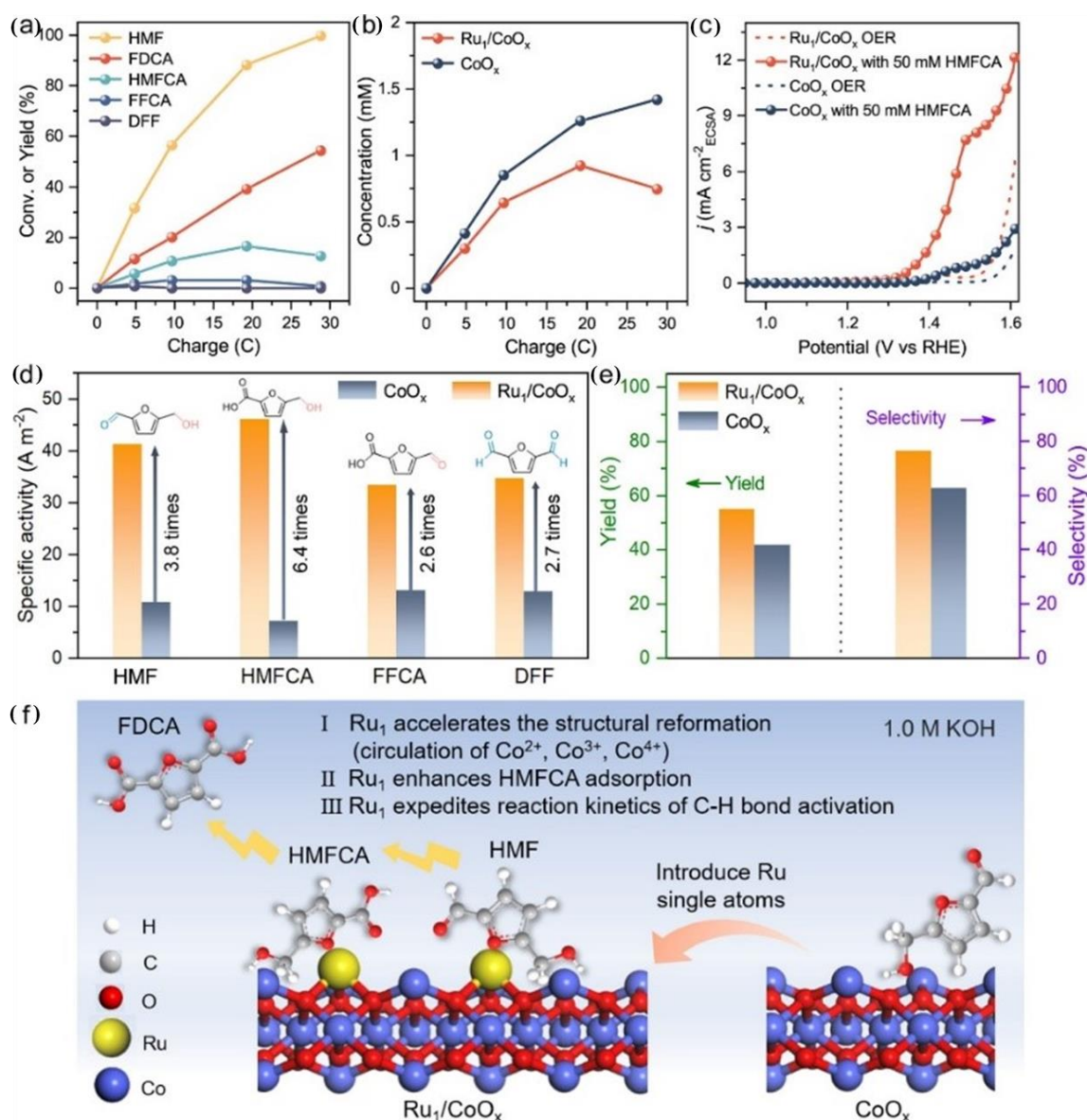


Figure 5. Identification of the reaction process and mechanism of CoO_x and Ru_1/CoO_x for HMFOR. (a) Conversion of HMF and the yields of oxidation products for Ru_1/CoO_x at different charges passed at the potential of 1.45 V vs. RHE in 1.0 M KOH with 5 mM HMF. (b) Concentration of HMFCFA during HMFOR for Ru_1/CoO_x and CoO_x at the potential of 1.45 V vs. RHE in 1.0 M KOH with 5 mM HMF. (c) ECSA-normalized LSV curves of CoO_x and Ru_1/CoO_x in 1.0 M KOH with/without 50 mM

HMFCA. (d) Specific activity of Ru_1/CoO_x and CoO_x at the potential of 1.45 V vs. RHE in 1.0 M KOH with 50 mM HMF, 50 mM HMFCA, 50 mM FFCA, and 50 mM DFF. (e) Yield and selectivity of FDCA of Ru_1/CoO_x and CoO_x after HMFOR transferring 28.9 C charge at the potential of 1.45 V vs. RHE in 1.0 M KOH with 5 mM HMF. (f) Scheme of the reaction process and mechanism of Ru_1/CoO_x and CoO_x . Reproduced from Ref. [22]. Copyright 2023, with permission from American Chemical Society.

Recently, Guo and co-workers designed a kind of Rh-O₅/Ni(Fe) atom site anchored on a nanoporous network with an NiFe-layered double hydroxide (Rh-SA/NiFe NMLDH) catalyst (Figure 6) [23]. The catalyst demonstrated exceptional performance for HMFOR, achieving an impressively low initial potential of 1.2 V and a current density of 50 mA cm⁻² at a voltage of 1.3 V. HMF conversion was 98%, the yield of FDCA was 99.8%, and the FE was 98.5% (Table 1, entry 13). In addition, the electrolytic cell assembled by Rh SA/NiFe NMLDH only needed a low voltage of 1.48 V to reach a current density of 100 mA cm⁻², and the durability was more than 100 h. DFT theoretical calculation results showed that the interaction between Rh and adjacent Ni atoms in the Rh-O₅/Ni(Fe) atomic structure optimized the electronic structures of Rh-4d and Ni-3d, and the electron transfer barriers between the active site and the key intermediates HMF and *OH were reduced respectively. The improvement of these synergistic effects was conducive to the electron exchange and transfer of HMFOR, and reduces the reaction energy barrier. Similarly, Li and co-workers exploited a two-step electrodeposition method to support single Ru atoms on NiFe LDH [24]. The synthesized $\text{Ru}_{0.3}/\text{NiFe}$ catalyst showed excellent HMF conversion (99.43%), FDCA selectivity (99.24%) and yield (98.68%) (Table 1, entry 14). It was found that Ru loading enhanced the reaction pathway from HMF to DFF, which improved the yield of FDCA. The experimental results and DFT calculation results showed that increasing the composition of Ru can optimize the adsorption energy of HMF and make FeNiOOH capture protons and electrons more effectively in HMFOR.

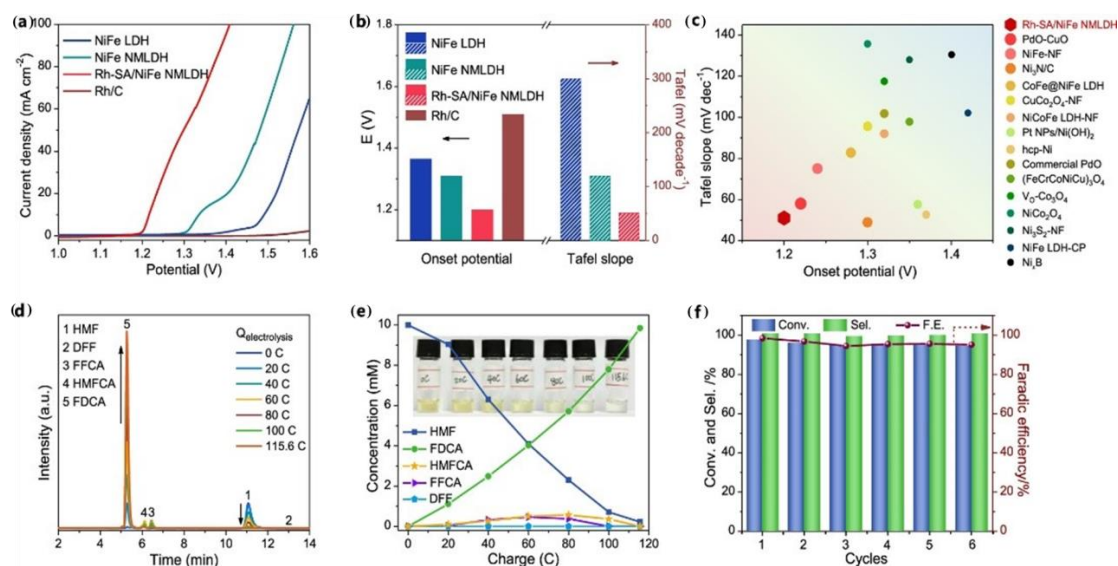


Figure 6. Electrocatalytic HMFOR performance. (a) Polarization curves in 1 M KOH with 0.05 M HMF solutions. (b) Activity comparison of onset potential at 2 mA cm² and Tafel slope for various catalysts. (c) Activity comparison among various representative catalysts reported in the literature involving the onset potential and potential at 50 mA cm². (d) High-performance liquid chromatography chromatograms obtained at various electrolysis charges. (e) Concentration versus charge plot of HMF, FDCA, and the intermediates at various electrolysis charges. Inset, the digital photos taken at different electrolysis charges. (f) Conversion, selectivity, and Faradaic efficiency toward HMFOR over six successive electrolysis cycles. Reproduced from Ref. [23]. Copyright 2023, with permission from American Chemical Society.

In general, the catalytic performance of the noble metal catalysts was less desirable due to factors such as a prolonged reaction time, low HMF conversion and low FDCA product yield, as well as the high cost of the noble metals. These factors were not favorable for large-scale production.

3.2. Non-Noble Metal Catalysts

Over the past few years, non-noble metal catalysts have gained significant popularity in the field of HMFOR research due to their cost-effectiveness and good electrical conductivity [7,31].

3.2.1. Non-Noble Metal Phosphides, Sulfides, Borides, and Nitrides

Heteroatom doping is an effective method to enhance the activity of non-noble metal electrocatalysts. In general, this strategy modulates the electronic structure of the catalyst by introducing non-metallic elements such as P, S, B, and N to change the chemisorption strength of the reactants, thus improving the HMFOR activity [31]. Table 2 summarizes recent advances in the electrocatalytic oxidation of HMF to synthesize FDCA using non-noble metal phosphide, sulfide, boride, and nitride catalysts.

Phosphides

In recent years, metal phosphides have attracted widespread attention in various small organic molecule electro-oxidation reactions such as HMF, methanol, ethanol, and ethylene glycol due to their excellent catalytic activity [32]. In 2016, Sun's research group first proposed the use of the metal phosphide catalyst Co-P/CF for HMFOR [33]. The Co-P was supported on a copper foam substrate by electrodeposition. The Co-P/CF catalyst could catalyze the oxidation of 50 mM HMF in 1.0 M KOH alkaline medium. The conversion rate of HMF was close to 100%, the yield of FDCA was about 90%, and the FE was 93%. Similarly, Sun and co-workers developed a Ni₂P NPA/NF catalyst loaded with Ni₂P nanoparticles on nickel foam, which also showed excellent catalytic activity for HMFOR [34]. The conversion rate of HMF was almost 100%, the FDCA yield was 98%, and the FE >98%. Afterwards, similar metal phosphide catalysts emerged one after another. In 2019, Li and co-workers developed a NiP-Al₂O₃/NF catalyst embedded in a two-dimensional amorphous alumina array on nickel foam to disperse Ni₂P, which could achieve 97.8% conversion of HMF and a 99.6% yield of FDCA [35].

Zhang and co-workers developed a metal-phytic acid hybrid Ni-PA catalyst using the biomass derivative phytic acid as a raw material, which demonstrated impressive catalytic performance for HMFOR [36]. The catalyst accomplished the full conversion of HMF, with an FDCA yield of 99.1% and an FE >90%. Recently, Menezes and co-workers developed an amorphous nickel-based NiP/NF catalyst synthesized by a one-step molecular method at room temperature, which could be reconstructed into a highly active nickel oxide phase (γ -NiOOH) during the HMFOR process [37]. This catalyst could achieve the electrocatalytic oxidation of 100 mM HMF in 1.0 M KOH alkaline medium with an HMF conversion rate of 96%, an FDCA yield of approximately 96%, and an FE of 96%. Seifitokaldani and co-workers developed a NiP@Ni/C catalyst by the cathodic deposition of nickel on a carbon paper substrate coated with a thin nickel film [38]. This catalyst exhibited remarkable activity for HMFOR, achieving an HMF conversion rate of over 90%, an FDCA yield of over 90%, and a Faradaic efficiency of 97%. Analysis indicates that the remarkable activity of the catalyst originated from highly oxidized nickel species on the surface of NiP. Xiong and co-workers prepared a phosphorus-engineered perovskite-oxide-derived LN-400-P-350 electrocatalyst through hydrothermal and phosphorization methods [39]. This catalyst could effectively electro-oxidize HMF in alkaline medium, achieving close to a 100% HMF conversion rate with an FDCA yield and an FE exceeding 90%. Furthermore, experimental and in situ Raman results demonstrated that the metal (oxy)hydroxide (NiOOH) was the true catalytic species.

Table 2. HMFOR catalyzed by non-noble metal phosphides, sulfides, borides, and nitrides ^a.

Type	Catalyst	HMF (mM)	Potential (V vs. RHE)	HMF Conversion (%)	FDCA Yield (%)	FE (%)	Ref.
Phosphides	Co-P/CF	50	1.423	~100	~90	93	[33]
	Ni ₂ P NPA/NF	10	1.423	~100	98	>98	[34]
	NiP-Al ₂ O ₃ /NF	0.3	1.45	97.8	99.6	-	[35]
	Ni-PA	10	1.60	100	99.1	90	[36]
	NiP/NF	100	1.49	96	96	96	[37]
	NiP@Ni/C	15	1.42	>90	>90	97	[38]
	LN-400-P-350	10	1.49	~100	~100	>90	[39]
	Ce-CoP	10	1.44	100	98	96.4	[40]
	Ce-Co ₂ P@NC	10	1.20	99.5	99.3	98.5	[41]
	CoNiP-NIE	10	1.50	-	-	87.2	[32]
	Mn-5Ni ₂ P	10	1.43	100	98	97.8	[42]
	Mn-FePSe ₃ /NS	10	1.30	98.8	-	92	[43]
CoMoP	100	1.36	99.9	95.8	93	[44]	
Sulfides	Ni ₃ S ₂ /NF	10	1.423	98	98	100	[45]
	Ni ₂ S ₃ /NF	10	1.498	100	98	94	[46]
	S-Ni@C	10	1.473	~100	96	96	[47]
	NiCo-S	10	1.45	99.1	97.1	96.4	[48]
	Co _{0.4} NiS@NF	10	1.45	100	>99	>99	[49]
	Co ₂ NiS	10	1.45	84.5 ^b	54 ^b	-	[50]
	Mn _{0.2} NiS/GF	100	1.48	99.3	97.6	94.2	[51]
	Cu-Ni ₃ S ₂ -R	20	1.40	~100	~100	~100	[52]
W ₂₀ -Ni ₃ S ₂ @NF	10	1.42	100	99.2	97.3	[53]	
Borides	Ni _x B/NF	10	1.45	100	98.5	~100	[54]
	NiB _x	10	1.426	≥99	≥99	≥99	[55]
	NiB _x -P _{0.07}	10	1.464	>99 ^b	90.6 ^b	92.5 ^b	[56]
Nitrides	Ni ₃ N@C	10	1.45	-	98	99	[57]
	Ni ₃ N	50	1.47	92	92	-	[58]
	Co ₄ N/NC@CC	10	1.38	99.2	98.6	97.8	[59]

^a The electrocatalytic oxidation of HMF was tested in 1.0 M KOH. ^b 0.1 M KOH.

The element doping or vacancy engineering of elements can regulate the electronic structure, surface characteristics, and conductivity of catalysts, thereby enhancing the activity of active sites and promoting the kinetic processes of electrocatalytic reactions [10,31]. Li and co-workers developed porous Ce-doped CoP nanosheets (Ce-CoP) through a deep eutectic solvent (DES) method [40]. The electrochemical conversion rate of HMF reached 100%, with an FDCA yield of 98% and a Faradaic efficiency of 96.4%. DFT theoretical calculations revealed that Ce doping and P vacancies caused significant electron redistribution in the CoP crystal, with electrons transferring from Ce atoms to P vacancies, resulting in electron accumulation in P vacancies and hole accumulation on Ce atoms. The hole accumulation on Ce atoms facilitated the adsorption of HMF, thereby promoting HMFOR. Similarly, Shen and co-workers prepared Ce-doped ultra-small Co₂P nanoparticles anchored on nitrogen-doped carbon nanosheets, forming the Ce-Co₂P@NC catalyst [41]. It demonstrated an electrochemical conversion rate of 99.5% for HMF, an FDCA yield of 99.3%, and a Faradaic efficiency of 98.5%. Experimental and DFT theoretical calculation results indicated that Ce doping effectively promoted the electron transfer of Co-based active species and the adjustment of the electronic band structure, thereby reducing the reaction energy barrier for the rate-determining step of HMFOR. Shao and co-workers reported a CoNiP-integrated electrode (CoNiP-NIE) for the catalytic oxidation of HMF, achieving an FE of 87.2% [32]. In situ potential-dependent electrochemical impedance spectroscopy (EIS) and Raman spectroscopy were used to detect the dynamic changes in the structure of the CoNiP catalyst. The research showed that during the catalytic process, CoNiP was initially oxidized to metal hydroxides, which were subsequently reduced in situ by HMF. DFT theoretical calculations also confirmed that CoNiP effectively enhanced the conductivity and moderate desorption of FDCA molecules, which were the main reasons for its high catalytic activity. Li and co-workers designed a novel Mn-doped Ni₂P electro-

catalyst (Mn-5Ni₂P) using microwave-assisted DES and phosphorization processes, which exhibited excellent catalytic activity for HMFOR with an HMF conversion rate of 100%, an FDCA yield of 98.0%, and a Faradaic efficiency of 97.8% [42]. DFT calculations showed that Mn doping not only effectively regulated the electronic structure of Ni, promoting HMF adsorption on Ni sites, but also provided new Mn-based adsorption sites. Liu and co-workers developed Mn-doped FePSe₃ nanosheets as a catalyst (Mn-FePSe₃/NS), with an HMF conversion rate of 98.8% and an FE of 92% [43]. DFT calculations demonstrated that Mn doping could facilitate HMF adsorption and lower the reaction barrier, thus accelerating the oxidation reaction.

Recent studies have found that heteroatom doping can change the crystal environment of catalytic materials and enhance the adsorption behavior of active intermediates by using the filling characteristics of d orbitals, so as to improve the performance of catalytic materials [8]. Tao and co-workers doped Mo onto CoP to induce lattice expansion to enhance the electro-oxidation of 100 mM HMF in 1.0 M KOH alkaline medium (Figure 7), resulting in a 99.9% HMF conversion, 95.8% FDCA yield, and 93% FE [44]. DFT theoretical calculations confirmed that the incorporation of Mo could improve the d-band center of Co in CoMoP and enhance the adsorption of HMF on the surface of CoMoP. At the same time, there are plenty of oxygen defects on the surface of CoMoP, and OH[•] can fill the defect sites, thus promoting the oxidation of low-valence metal ions and finally obtaining high-oxidation-state substances in the synergistic catalysis of HMFOR. In addition, the surface-reconstructed Mo-O and CoOOH are the active sites for the initial oxidation of hydroxyl.

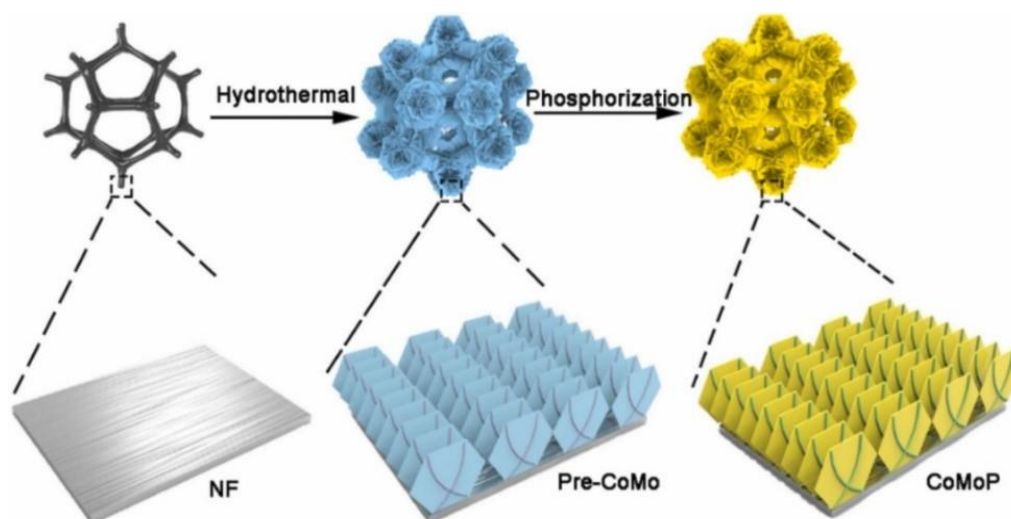


Figure 7. Schematic diagram of the synthesis of CoMoP. Reproduced from Ref. [44]. Copyright 2023, with permission from Elsevier.

Sulfides

In 2016, Sun and co-workers first reported the application of non-noble metal sulfides in HMFOR [45]. Ni₃S₂/NF catalyst with hierarchical porous structure could achieve an HMF conversion of 98%, an FDCA yield of 98%, and an FE of 100%. Similarly, Wang and co-workers reported a Ni₂S₃/NF catalyst prepared by the hydrothermal sulfuration method, which achieved nearly a 100% HMF conversion, a 98% FDCA yield, and a 94% FE [46]. In addition, Wang and co-workers also used lignin sulfonate (LS), a pulp industrial waste, as a carbon and sulfur precursor to prepare S-Ni@C-600 catalyst by hydrothermal reaction and carbothermal reduction [47]. The catalyst could achieve the almost complete conversion of HMF, with an FDCA yield of 96% and an FE of 96%. The results showed that nickel hydroxide on the surface and carbon shell were helpful to improve the electrocatalytic activity.

The construction of bimetallic sites and the adjustment of coordination substances are considered to be effective strategies to improve the performance of HMFOR [48].

Zheng and co-workers constructed layered nickel-based sulfide nanosheets (NiCo-S) for HMFOR [48]. The conversion of HMF was 99.1%, the yield of FDCA was 97.1%, and the FE was 96.4%. Electrochemical experiments and theoretical results showed that Ni-Co dual sites cooperatively participated in HMFOR, in which Co sites promoted the conversion of the HMF aldehyde group to a carboxyl group and had strong diatomic adsorption (O and C atoms) on the aldehyde group, while Ni sites could accelerate the generation rate of FDCA. Similarly, Wang and co-workers developed a $\text{Co}_{0.4}\text{NiS@NF}$ catalyst; the HMF conversion was 100%, the FDCA yield was >99%, and the FE was >99% [49]. It was found that Co doping not only helped to expose more active sites, but also effectively regulated the electronic properties of Ni_3S_2 and promoted electron/charge transfer and/or rapid mass transfer processes, thereby improving the activity for HMFOR. Peng and co-workers also found that doping Co could reduce the overpotential of HMFOR and promote the formation of high-valence nickel. Co and Ni in the Co_2NiS catalyst synergistically promoted HMFOR [50]. Recently, Wang and co-workers synthesized an Mn-doped NiS nanosheet electrocatalyst $\text{Mn}_{0.2}\text{NiS}/\text{GF}$ on a 3D graphite felt (GF) substrate [51]. This catalyst had excellent HMFOR activity with an HMF conversion of 99.3%, FDCA yield of 97.6%, and FE of 94.2%. The research shows that both Mn and Ni can be used as adsorption sites for HMFOR. Mn doping not only provides new adsorption sites for HMF, but also promotes the formation of nanosheet arrangement and increases the number of active sites, thus promoting HMFOR.

Recently, Zheng and co-workers used the strategy of combining surface reconstruction and heteroatom doping (Cu, Fe, V, and Zn) to modify the Ni_3S_2 precatalyst to prepare a series of M/ Ni_3S_2 -R catalysts (Figure 8) [52]. It was found that Cu^{2+} ($3d^9$) with its unique electronic structure provided abundant Lewis acid sites for HMF adsorption. Successful doping and surface reconstruction adjusted the local coordination environment of active Ni sites and accordingly adjusted the d-band center, improved the electrocatalytic activity, and thus promoted the reaction kinetics. DFT calculation results showed that the ideal adsorption of OH and HMF and better conductivity of Cu/ Ni_3S_2 -R were the reasons for improving the electrocatalytic oxidation activity. Cu/ Ni_3S_2 -R exhibited the best HMFOR performance with a nearly 100% HMF conversion, nearly 100% FDCA yield, and nearly 100% FE. Yan and co-workers prepared a W-doped Ni_3S_2 nanocatalyst ($\text{W}_{20}\text{-Ni}_3\text{S}_2\text{@NF}$) by hydrothermal synthesis and low-temperature sulfurization calcination [53]. It is found that W doping could expose more active sites and improve the conductivity of Ni_3S_2 . More importantly, W doping effectively controlled the adsorption of HMF and OH^* . In addition, the addition of high-valence W caused the d-band center of Ni_3S_2 to shift upward, which was conducive to the adsorption and dissociation of water to produce more OH^* . Moreover, the high-valence W had a strong electron-withdrawing ability and led to the increase in the Ni valence state by attracting electrons in Ni, which was conducive to optimizing the adsorption energy of HMF. These factors together accelerated the dynamics of HMFOR and had excellent HMFOR performance. The results showed that the $\text{W}_{20}\text{-Ni}_3\text{S}_2\text{@NF}$ catalyst had a 100% HMF conversion, 99.2% FDCA selectivity, and 97.3% FE.

Borides

In 2018, Schuhmann and co-workers reported the use of nickel foam modified with high-surface-area nickel boride $\text{Ni}_x\text{B}/\text{NF}$ as electrode [54]. HMF was completely converted with an FDCA yield of 98.5% and an FE close to 100%. The products and intermediates were analyzed by electrochemical-coupled attenuated total reflection infrared spectroscopy (EC-ATR-IR) for the first time. It was found that the oxidation of HMF was through HMFC intermediates rather than the DFF pathway.

Subsequently, in 2019, Sun and co-workers developed a paired electrolysis system using NiB_x as a catalyst for anodic HMFOR and the cathodic hydrogenation of *p*-nitrophenol (*p*-NP) to produce *p*-aminophenol (*p*-AP) [55]. This paired electrolytic cell used electricity to drive organic oxidation and hydrogenation reactions in aqueous solutions, without the need to handle hazardous gaseous hydrogen or oxygen or add external oxidants/reducing

agents. The experimental results indicated that the electrogenerated Ni^{3+} was an active intermediate. Using water as an oxygen and hydrogen source, the conversion, efficiency, selectivity, and FE on both sides were all $\geq 99\%$ (Figure 9).

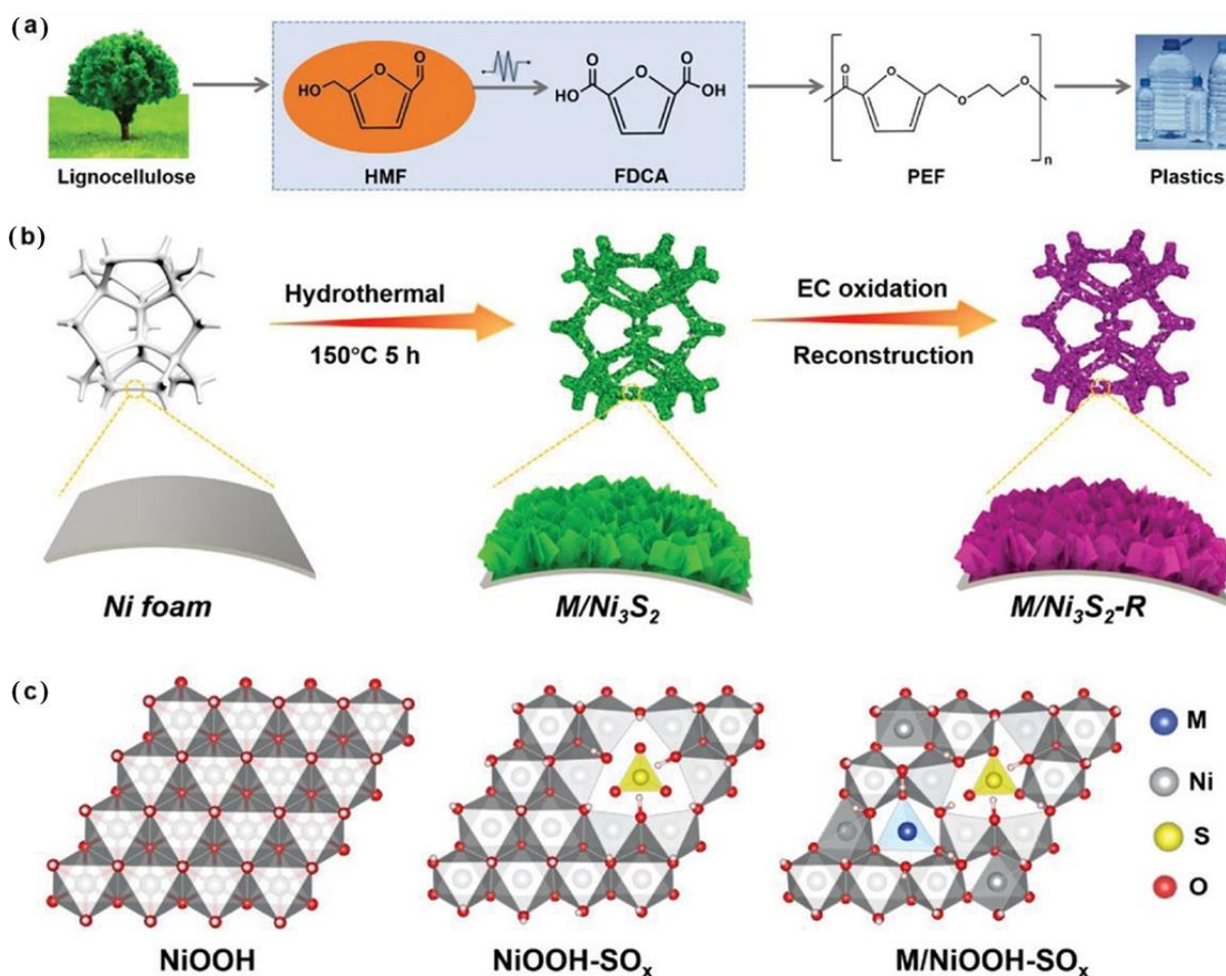


Figure 8. (a) Biomass-derived PEF route for the plastic industry. (b) Schematic illustration for the synthesis of $\text{M}/\text{Ni}_3\text{S}_2\text{-R}$ electrocatalysts ($\text{M} = \text{Fe}, \text{Zn}, \text{V}, \text{and Cu}$). (c) Optimized structural models of NiOOH , oxysulfide-coordinated NiOOH (NiOOH-SO_x , termed $\text{Ni}_3\text{S}_2\text{-R}$), and oxysulfide-coordinated transitional metal-doped NiOOH ($\text{M}/\text{NiOOH-SO}_x$, termed $\text{M}/\text{Ni}_3\text{S}_2\text{-R}$). Reproduced from Ref. [52]. Copyright 2023, with permission from Wiley.

In 2020, Wang and co-workers synthesized phosphorus-doped nickel boride ($\text{NiB}_x\text{-P}_y$) and investigated the effect of different phosphorus dosages on the electrocatalytic performance of HMFOR [56]. The results showed that with the increase in phosphorus content, the yield of FDCA on the $\text{NiB}_x\text{-P}_y$ catalyst was first increased and then decreased. The electrocatalytic performance of the $\text{NiB}_x\text{-P}_{0.07}$ catalyst was the best with the highest FDCA yield of 90.6% and FE reaching 92.5%, while the FDCA yield and FE of the undoped NiB_x catalyst were 75.5% and 80.1%, respectively. In addition, research has found that phosphorus doping promotes the electron transfer of nickel and the generation of nickel hydroxide species (NiOOH), which are the true catalytic active substances for HMFOR, thereby improving the electrocatalytic performance of HMFOR.

Recently, Xiao and co-workers used initial principle calculations to systematically study the catalytic performance and reaction mechanism pathways of Mo_2B_2 MBene in HMFOR [60]. The results indicated that Mo_2B_2 MBenes could effectively convert HMF into FDCA with a limit potential of $-0.49/\text{eV}$.

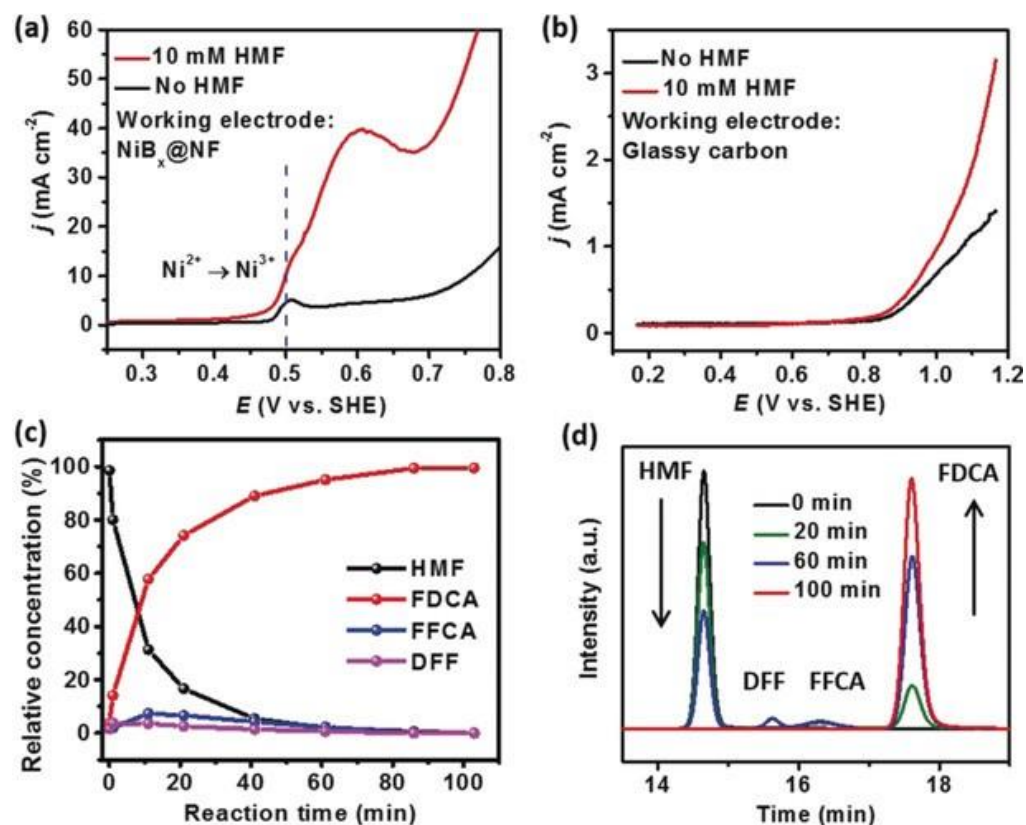


Figure 9. (a) LSV curves for NiB_x@NF in 1 M KOH with and without HMF (10 mM); (b) LSV curves for a glassy carbon plate in 1 M KOH with and without 10 mM HMF (scan rate, 5 mV s⁻¹); (c) concentration of HMF, FDCA, and intermediates versus electrolysis time; (d) HPLC chromatograms acquired at various electrolysis times. Reproduced from Ref. [55]. Copyright 2019, with permission from Wiley.

Nitrides

In 2019, Wang and co-workers first reported the use of non-noble metal nitrides for HMFOR. They designed and prepared a carbon-coated nickel nitride Ni₃N@C catalyst by a hydrothermal and nitridation process [57]. The FDCA yield reached a maximum of 98%, and the FE reached 99%. It was found that the introduction of carbon could enable Ni₃N to form nanosheets instead of aggregated large particles and effectively regulate the electron distribution on the surface of Ni₃N, thereby improving the catalytic activity of HMFOR. In addition, for the first time, in situ sum frequency generation (SFG) technology was used to investigate the oxidation reaction pathway of HMFOR (Figure 10). It was found that HMF was first oxidized to the intermediate HMFCa at 1.35 V, and after the potential increased to 1.45 V, the intermediate continued to be oxidized to FDCA. Therefore, the catalytic reaction pathway of Ni₃N@C is HMFCa.

In 2021, Wang and co-workers further explored the activity sources of Ni₃N catalysts for HMFOR and the influence of electrolyte alkalinity through various in situ characterization techniques [58]. Results showed that the active source of the Ni₃N catalyst was Ni^{2+δ}N(OH)_{ads} and a two-step reaction was proposed to explain the HMFOR process. Firstly, applying an electric potential will cause Ni atoms to lose electrons and adsorb OH⁻, binding with electrophilic oxygen to form Ni^{2+δ}N(OH)_{ads}. Then, the electrophilic oxygen in Ni^{2+δ}N(OH)_{ads} takes protons and electrons from HMF and spontaneously transforms into H₂O. In addition, a higher electrolyte alkalinity will promote the formation of Ni^{2+δ}N(OH)_{ads} and the adsorption of HMF on the Ni₃N electrode.

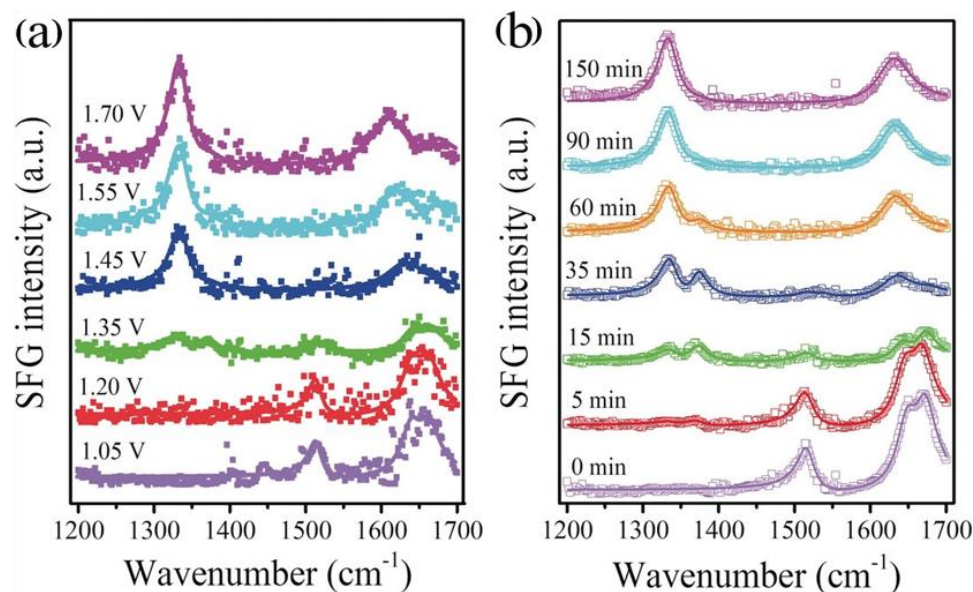


Figure 10. SFG spectra with ssp polarizations recorded at the working electrode/electrolyte interface (a) after running the cell at various voltages for 90 min and (b) by monitoring the reaction at different times at 1.45 V vs. RHE in 1 M KOH and 20 mM HMF. The “ssp” is the polarization direction of the light source. Reproduced from Ref. [57]. Copyright 2019, with permission from Wiley.

The synthesis of metal nitrides usually involves multi-step reactions and requires calcination under NH₃ atmosphere. Recently, Wang and co-workers developed nitrogen-doped carbon composite Co₄N ultra-thin nanosheets self-supporting electrodes (Co₄N/NC@CC) on carbon cloth by the deep eutectic solvent (DES) method without the use of NH₃ [59]. This catalyst exhibited good catalytic activity for HMFOR with a conversion rate of 99.2% for HMF, a selectivity of 98.6% for FDCA, and an FE of 97.8%. It was found that the strong interaction between Co₄N and NC accelerated electron transfer at the interface. The ultra-thin nanostructure of Co₄N/NC was beneficial for increasing the catalytic active sites, thereby effectively improving the catalytic performance.

3.2.2. Non-Noble Metal Hydroxides and Oxides

Numerous investigations have revealed that the non-noble metal hydroxides/oxides in a high-valence state are likely to be the catalytic active centers in a strong alkaline electrolyte [3,5]. Therefore, the direct design and development of non-noble metal hydroxides and oxides catalysts will help to understand the intrinsic activity of catalysts for HMFOR and to develop more efficient catalysts for future applications. Table 3 summarizes recent advances in the electrocatalytic oxidation of HMF to synthesize FDCA using non-noble metal hydroxide and oxide catalysts.

Hydroxides

In recent years, the earth-abundant transition metal hydroxides catalysts have been favored by many scientists, especially bimetallic layered double hydroxides (LDHs), which are hydrotalcite analogues [3]. Due to the exposed metal centers in their structures playing a coordinating role, they can reduce the energy barrier of the electrochemical reaction and improve the conductivity of electrolyte ions, further accelerating the electrochemical reaction kinetics. Early research found that NiFe LDHs exhibited excellent catalytic activity in electrocatalytic water oxidation (OER) [31,61,62]. Subsequently, researchers tried to apply it to HMFOR [63]. In 2018, Huber and co-workers constructed NiFe LDH nanosheets grown on carbon fiber paper [64]. This was the first attempt to use bimetallic LDHs as anode material in the direct electrochemical oxidation of HMF to FDCA. Compared with other Ni-based catalysts (NiAl LDH, NiGa LDH, and Ni(OH)₂), NiFe LDH has the best catalytic activity. The conversion of HMF was 99%, the selectivity of FDCA was 98%, and

the FE was 99.4%. The results showed that the introduction of Fe increased the number of active sites, which improved the catalytic activity for HMFOR. Subsequently, many metal LDH electrode materials were developed.

In 2020, Yan and co-workers prepared ternary hydrotalcite ultra-thin NiCoFe-LDH nanosheets by the coprecipitation method and applied it to HMFOR [65]. It was found that compared with NiCo-LDHs and NiFe LDHs, the NiCoFe-LDHs nanosheets had ultra-thin thickness, which was only ~1.36 nm. This showed that the introduction of Fe ions could change the metal layer and reduce the barrier effect of the layer. Therefore, the nanosheets will not accumulate during the synthesis process, resulting in an ultra-thin structure that is conducive to improving the ion transport in the electrocatalytic process. In addition, the NiCoFe-LDHs catalyst showed excellent HMFOR performance. The overpotential of NiCoFe-LDHs at 10 mA cm⁻² was 300 mV, and the Tafel slope was 68 mV dec⁻¹. The HMF conversion exceeded 95% and a nearly 85% FDCA selectivity was obtained within one hour.

Although LDHs have attracted extensive attention due to their diverse cationic composition, adjustable electronic structure, and simple preparation methods, they lack accessible active sites and have low conductivity. Recent studies have shown that it is helpful to improve the HMFOR performance by implanting metal vacancies to change the electronic configuration and metal site coordination environment of LDHs [66]. In 2022, Wang and co-workers prepared a kind of d-NiFe LDH/CP catalyst with cation rich defects by hydrothermal and alkali etching methods [66]. A series of physical characterization studies confirmed the successful removal of zinc and the introduction of cationic vacancies. The catalyst showed excellent catalytic activity. At 1.48 vs. RHE potential, HMF was almost completely converted (97.35%), the yield of FDCA was 96.8% and FE was 84.47%. After 10 cycles, the catalytic performance was still maintained. The results showed that the introduction of abundant cationic vacancies was the main reason for the high catalytic activity, which significantly adjusted the electronic structure of the NiFe LDH. The electrochemical active surface area was greatly increased, and the charge transfer resistance was reduced. In addition, the metal (oxygen) hydroxides formed in situ were active substances. This work provided ideas for the design of defect-rich catalysts and their application to the upgrading of biomass derivatives by electrochemical oxidation.

Recent studies have found that coupling LDHs with other conductive nanomaterials to construct self-supporting electrodes is a simple and effective method, which can improve the active surface area and conductivity of LDHs. For example, Fan and co-workers prepared a Ni_xSe_y-NiFe LDH@NF electrocatalyst with 3D layered core-shell structure and its application to HMFOR [67]. It was found that the Ni_xSe_y nanowire core with high conductivity accelerated charge transfer and had good mechanical strength. The NiFe LDH nanosheets as the shell with a large specific surface area provided abundant active sites, and the layered nanoarray structure was conducive to the diffusion of electrolytes. In addition, NiOOH was the main active site, and Fe could adjust the electronic structure of Ni to improve the catalytic activity. Thanks to the above advantages, the Ni_xSe_y-NiFe LDH@NF core-shell catalyst showed excellent catalytic performance for HMFOR. The high yield of FDCA was 99.3%, the FE was as high as 98.9%, and the FE remained at 96.7% after six consecutive electrolytic cycles. Similarly, Li and co-workers developed an NiFe LDH/CoCH/NF electrocatalyst by a two-step hydrothermal method [68]. Compared with NiFe LDH/NF and CoCH/NF, the coupled NiFe LDH/CoCH/NF catalyst had a unique folded nanosheet structure and a higher electrochemical active surface area, faster electron transfer kinetics, and more active sites. The oxidation conversion of HMF was 98.8%, the yield of FDCA was 98.6%, and the FE was 98.1%.

Table 3. HMFOR catalyzed by non-noble metal hydroxides and oxides ^a.

Type	Catalyst	HMF (mM)	Potential (V vs. RHE)	HMF Conversion (%)	FDCA Yield (%)	FE (%)	Ref.
hydroxides	NiFe LDH	10	1.23	99	98	99.4	[64]
	NiCoFe LDHs	10	1.54	95.5 ^b	84.9 ^b	~90 ^b	[65]
	d-NiFe LDH/CP	10	1.48	97.35	96.8	84.47	[66]
	Ni _x Se _y -NiFe LDH@NF	10	1.423	99.6	99.3	98.9	[67]
	NiFe LDH/CoCH/NF	5	1.58	98.8	98.6	98.1	[68]
	Ni ₃ V ₁ -LDHs	100	-	83.5	79.5	-	[69]
	CF-Cu(OH) ₂	100	0.8	~100	98.7	~100	[70]
	14%Ce-Ni(OH) ₂	10	0.45	100	-	86.6	[71]
	Cr-Ni(OH) ₂ /NF	10	1.47	~100	>98	-	[72]
oxides	CoNW/NF	100	1.504	100	96.8	96.6	[73]
	mesoporous δ-MnO ₂	10	1.35	100	98	98	[74]
	CuMn ₂ O ₄	10	1.31	100	-	96	[75]
	CuCo ₂ O ₄	50	1.45	-	93.7	94	[76]
	BiCoO-NA/NF	10	1.30	~100	-	97.7	[77]
	Co ₃ O ₄ -VO	5	1.52	90	61	56	[78]
	N-Co ₃ O ₄ /NF-2	10	1.423	99.5	96.4	97.3	[79]
	CoO _x H _y -MA	5	1.52	-	98	83	[80]
	NiO-N/C	10	1.473	99	84	96	[81]

^a The electrocatalytic oxidation of HMF was tested in 1.0 M KOH. ^b 1.0 M NaOH.

In addition to the widely studied Ni-, Co-, and Fe-based LDHs, V-based LDHs (such as NiV-LDHs) are composed of lower-cost V elements, which can exhibit excellent intrinsic catalytic activity due to their excellent conductivity, fast electron transfer, and abundant active sites. Recently, Yan and co-workers developed ultra-thin NiV layered double metal hydroxide films (NiV-LDHs) for the efficient electrocatalytic oxidation of a variety of biomass aldehyde platform molecules [69]. The results showed that the Ni₃V₁-LDHs film with the thinnest thickness (2.6 nm) had rich active sites, which was conducive to the adsorption of aldehydes and the generation of hydroxyl radicals to oxidize a variety of biomass aldehyde platform molecules such as benzaldehyde, multi-site methoxybenzaldehyde, furfural, and HMF. The experimental results and theoretical calculations showed that NiV-LDHs could produce abundant hydroxyl radicals on the surface and promote the formation of FDCA. The oxidation conversion of HMF was 83.5%, and the yield of FDCA was 79.5%.

Fan and co-workers prepared a CF-Cu(OH)₂ catalyst by growing Cu(OH)₂ in situ on foam copper for HMFOR [70]. It was found that CF-Cu(OH)₂ electroactivation produced CuOOH active substances, which were the main catalytic sites for HMFOR. In addition, electrochemical performance tests showed that the current density of CF-Cu(OH)₂ reached 198.2 mA cm⁻² (100 mM HMF, 1.0 M KOH, 0.8 V vs. Ag/AgCl). The HMF oxidation conversion and FE were close to 100%, and FDCA yield was 98.7%. In addition, it was demonstrated that the oxidation of HMF was achieved through a two-step oxygen transfer mechanism. Firstly, Cu(OH)₂ was electrochemically oxidized into highly oxidized CuOOH in alkaline solution, and then the active substance CuOOH further oxidized HMF into the corresponding products, as well as regenerating into Cu(OH)₂.

Recent studies have shown that the mismatched crystal structures of M(OH)₂ and MOOH can cause phase transitions during the catalytic process, which may result in the instability of M(OH)₂ catalysts and reducing their adsorption and activation ability for HMF molecules. Therefore, the HMFOR activity of a single hydroxide system is still insufficient at present [71]. The doping of guest ions is considered an effective method for buffering lattice transition. Meanwhile, the doped phase further endows new active sites. For example, recently, Fan and co-workers prepared a novel Ce-doped Ce-Ni(OH)₂ catalyst, which could be further oxidized and activated to Ce-NiOOH through electrochemical reconstruction strategy [71]. It was found that the introduction of Ce not only solved the problem of Ni(OH)₂ matrix collapse during the phase transition from Ni(OH)₂ to NiOOH, but also improved the reaction activity. The experimental results showed that the optimal current density for 14% Ce-Ni(OH)₂ was 27 mA cm⁻² (0.45 V vs. Ag/AgCl), and it could

still maintain excellent activity after the 50th cyclic voltammetry (CV) test. In addition, the catalyst significantly improved the reaction kinetics for HMFOR, which was beneficial for increasing the yield and Faradaic efficiency of FDCA. Similarly, Mou and co-workers compared the performance of nickel hydroxide modified with different metal elements (Co, Mn, Fe, Cr, Mo, and Ga) and focused on revealing the decisive role of the proton-coupled electron transfer (PCET) process in affecting the anode peak current [72]. The results showed that the HMF conversion current density of 230 mA cm^{-2} could be achieved at 1.47 V vs. RHE potential by growing the appropriate Cr-doped Cr-Ni(OH)₂/NF catalyst on the nickel foam substrate. Within 32 min, the HMF conversion was nearly 100% and the FDCA selectivity was more than 98%, and it remained stable after six cycles.

Oxides

In 2019, Zhang and co-workers developed hydrothermal and low-temperature pyrolysis methods to grow pine-needle-like Co₃O₄ nanowires (CoNW/NF) in situ on nickel foam [73]. The nanowire array has the defect characteristics of rich crystals and interconnected pores, making CoNW/NF show excellent HMFOR performance. It was found that the required potential was only 1.269 V at a current density of 10 mA cm^{-2} and the corresponding Tafel slope was 125 mV dec^{-1} , indicating that the synthesized CoNW/NF catalyst had high thermodynamic and kinetic activity. Importantly, the HMF oxidation conversion was 100%, the FDCA yield was 96.8%, and the FE was 96.6%. It had strong electrochemical durability for up to 30 h over five consecutive chronoamperometry experiments. Wu and co-workers prepared pure-phase mesoporous nanostructure δ -MnO₂ with a high surface area through a simple nanocasting method [74]. The catalyst can serve as an efficient selective catalyst for HMFOR under both alkaline and acidic conditions. Among them, under alkaline conditions, the mesoporous δ -MnO₂ catalyst had high activity and stability for HMFOR, and HMF could be completely converted. The yield of FDCA was as high as 98%, and the FE was as high as 98%.

In recent years, spinel type bimetallic oxides have received widespread attention due to their excellent catalytic performance, high stability, and unique crystal structure (coexistence of tetrahedral and octahedral sites) [76,82]. For example, in 2021, Lei and co-workers synthesized spinel CuMn₂O₄ with sea-urchin-like nanostructures using a hydrothermal method and then immersed it in ammonia to generate oxygen vacancies [75]. The results indicated that the ammonia-etched CuMn₂O₄ exhibited excellent HMFOR performance. At a current density of 20 mA/cm^2 , the oxidation potential of HMF was 1.31 V vs. RHE in a 1.0 M KOH solution. The conversion of HMF was 100%, and the FE of FDCA was 96%. Similarly, Wang and co-workers investigated the influence of geometric sites on the performance of HMFOR on cobalt spinel oxides (Co₃O₄, ZnCo₂O₄, and CoAl₂O₄) by constructing specific blocks on tetrahedral sites (Co²⁺_{Td}) and octahedral sites (Co³⁺_{Oh}), and discovered the importance of geometric sites [76]. The electrochemical performance was as follows: CoAl₂O₄ < ZnCo₂O₄ < Co₃O₄, indicating that octahedral CoO₆ had high catalytic activity. Based on the geometric position dependence found above, Cu²⁺ was introduced to cooperate the occupation of octahedral Co³⁺ in spinel oxides, significantly improving the oxidation activity of HMF. The FDCA yield was 93.7%, and the FE was 94%. Recently, Liu and co-workers synthesized a Bi-doped Co₃O₄ nanosheet (BiCoO-NA/NF) on nickel foam and investigated its performance for HMFOR [77]. Due to the synergistic effect between the layered structure and Bi doping, BiCoO-NA/NF could achieve approximately full conversion of HMF at a voltage of 1.3 V vs. RHE potential, with an FE of up to 97.7%. After 10 consecutive cycles, BiCoO-NA/NF showed good stability.

Controlling the electronic structure of materials through defect engineering is also an effective way to improve the performance of HMFOR [10,31]. In 2022, Huang and co-workers proposed a simple topological chemical transformation method to synthesize oxygen-enriched oxygen vacancies in Co₃O₄-VO nanosheets [78]. Compared to CoO_xH_y nanosheets and conventionally roasted Co₃O₄ nanosheets, the Co₃O₄-VO nanosheets exhibited higher HMFOR catalytic performance. The conversion of HMF was 90%, the yield of FDCA

was 61%, and the FE was 56%. The surface without surfactants and the well-preserved two-dimensional structure made it easier to obtain Co active sites. The abundant oxygen vacancies were conducive to the transfer of mass and charge. However, there is still room for improvement in the catalytic performance of Co_3O_4 -VO for HMFOR. Zhang and co-workers employed a controllable nitrogen-doping strategy to prepare N- Co_3O_4 /NF-2 catalysts [79]. N doping can induce the formation of oxygen vacancies, jointly regulate the electronic structure of the Co element, and improve the conductivity of Co_3O_4 . The obtained N- Co_3O_4 /NF-2 exhibited excellent catalytic activity for HMF oxidation. At a voltage of 1.423 V vs. RHE potential, the HMF conversion was 99.5%, the FDCA yield was 96.4%, and FE was 97.3%. N- Co_3O_4 /NF-2 also exhibited excellent catalytic durability and structural stability in HMFOR. Wang and co-workers prepared a nitrogen-modified nickel oxide catalyst NiO-N/C for HMFOR [81]. The HMF conversion of was 99%, the FDCA yield was 84%, and the FE was 96%. This catalyst had good stability and remained active even after six consecutive reactions. Recently, Huang and co-workers prepared a series of defective hydrated cobalt oxide nanosheets (CoO_xH_y) by using methylamine (MA) and/or NaBH_4 (BH) via room-temperature reduction methods [80]. These CoO_xH_y nanosheets with defect structures had abundant oxygen vacancies, high $\text{Co}^{2+}/\text{Co}^{3+}$ ratios, and high porosity. The ultra-thin layered framework significantly improved the catalytic activity and selectivity for HMFOR. In addition, the DFT theoretical calculation results indicated that the oxygen vacancies had a promoting effect on the adsorption and activation of HMF, especially through the aldehyde groups of HMF. With the optimal CoO_xH_y -MA catalyst, the FDCA yield reached 98% and the FE reached 83% within 200 min at a constant potential of 1.52 V vs. RHE.

3.2.3. Heterostructures

In recent years, interface engineering has been considered as an effective method for designing efficient electrocatalysts since electrocatalytic reactions typically occur at interfaces [10]. Heterostructures can promote electron transfer and influence the adsorption/desorption energies of active species in electrocatalytic reactions, thereby modulating the catalytic capabilities. Moreover, the synergistic effects between heterogeneous components may also contribute to further enhancing the catalytic activity and stability of heterostructures [8]. Table 4 summarizes recent advances in the electrocatalytic oxidation of HMF to synthesize FDCA using heterostructures catalysts.

In 2020, Fu and co-workers reported the synthesis of porous carbon-coated MoO_2 -FeP@C heterostructures through a synthetic strategy inspired by polyoxometalate-based metal-organic frameworks (POMOFs), using nano-spindle-shaped hydroxylated iron oxide (FeOOH) as a sacrificial substrate [83]. By introducing heteropolyacid (PMo_{12}) and organic ligands to the in situ formation of Mo-Fe organic complexes on FeOOH followed by controlled phosphorization, the synthesized MoO_2 -FeP@C exhibited abundant active interfaces. The results demonstrated electron redistribution at the interfaces of MoO_2 -FeP@C, with electron accumulation on FeP facilitating the optimized absorption of H_2O and H^* , thereby enhancing HER activity. Meanwhile, hole accumulation on MoO_2 favors the absorption of biomass-derived organic compounds. The catalyst showed outstanding HMFOR performance with an HMF conversion of 99.4%, FDCA yield of 98.6%, and FE of 97.8%. Additionally, various biomass derivatives, including benzyl alcohol (BA), furfural (FF), furfuryl alcohol (FFA), 4-nitrobenzyl alcohol (NBA), and 4-methoxybenzyl alcohol (MBA), were used as substitutes for HMF, and MoO_2 -FeP@C also exhibited excellent catalytic performances. Similarly, Zou and co-workers constructed a three-dimensional layered nanostructure of the NiO- Co_3O_4 electrocatalyst with abundant interfaces [84]. It was found that due to the different crystal structures of Co_3O_4 (spinel) and NiO (face-centered cubic), the atomic arrangement at the interfaces was not one-to-one, resulting in a large number of defects and vacancies. The interface effect produced abundant cation vacancies, altering the electronic properties of Co and Ni atoms and enhancing the oxidation state of Ni. The NiO- Co_3O_4 catalyst exhibited excellent HMFOR activity with an HMF conversion close

to 100%, FDCA yield up to 98%, and FE of 96% at 1.45 V vs. RHE potential. Han and co-workers reported a core-shell NiSe@NiO_x electrocatalyst for the conversion of HMF to FDCA [85]. It was found that NiSe@NiO_x consisted of conductive NiSe nanowires as the core, while the surface NiO_x shell played the role of the active sites. At 1.423 V vs. RHE potential, the HMF conversion was 98%, the FDCA yield was 96%, and the FE was 97%. In addition, X-ray photoelectron spectroscopy revealed that high-valence Ni species may serve as the active sites in the NiO_x shell.

Table 4. HMFOR catalyzed by heterostructures ^a.

Catalyst	HMF (mM)	Potential (V vs. RHE)	HMF Conversion (%)	FDCA Yield (%)	FE (%)	Ref.
MoO ₂ -FeP@C	10	1.424	99.4	98.6	97.8	[83]
NiO-Co ₃ O ₄	10	1.45	~100	98	96	[84]
NiSe@NiO _x	10	1.423	98	96	97	[85]
Ni ₃ N-V ₂ O ₃	10	1.40	97.4	96.1	-	[86]
CoP-CoOOH	150	1.42	98.3	96.3	96.3	[87]
Y-Co-CoS _x @CN	5	1.29	100 ^b	96 ^b	93.5 ^b	[88]
CoP/Ni ₂ P-NiCoP@NC-600	5	1.32	-	98.1 ^b	97.6 ^b	[89]
Ni(OH) ₂ -NiOOH/NiFeP	10	1.435	99.4	99.4	94.62	[90]
Ni ₃ N-NiMoN/CC	10	1.40	100	98	~100	[91]
t-Ni-P@POC	10	1.42	100	99.9	99.7	[92]
Co-Ni _x P@C	10	1.38	~100	~100	98.9	[93]
NF@Co ₃ O ₄ /CeO ₂	50	1.40	98	94.5	97.5	[94]
NF/Co ₄ N@CeO ₂	10	1.425	91.1	93.6	84.5	[95]
Cu ₂ P ₇ -CoP	10	1.43	100	98.8	98	[96]
NiS _x /Ni ₂ P	10	1.46	~100	98.5	95.1	[97]
NiFeP@NiFe(OH) _x	10	1.45	-	-	94.42	[98]
a-Ni(OH) ₂ -Cu ₂ O/NF-6	50	1.424	-	91	98	[99]
Ni/Ni _{0.2} Mo _{0.8} N/NF	50	1.423	~100	98.5	~100	[100]
Ni-VN/NF	10	1.402	>99	99	>98	[101]
NiCo ₂ @MoO ₂ -NF	10	1.40	~100	99.6	99.4	[102]
NiOOH-coated Cu(OH) ₂	5	1.40	100 ^c	98.3 ^c	98.3 ^c	[103]

^a The electrocatalytic oxidation of HMF was tested in 1.0 M KOH. ^b 0.1 M KOH. ^c 0.1 M NaOH.

In 2021, Yang and co-workers constructed a Ni₃N-V₂O₃ heterostructure catalyst and found that the interaction between Ni₃N and V₂O₃ resulted in electron transfer from Ni₃N to V₂O₃ [86]. The catalyst exhibited excellent catalytic performance for HMFOR, with an HMF conversion of 97.4% and FDCA yield of 96.1% at 1.40 V vs. RHE potential. In 2022, Tao and co-workers developed a porous CoP-CoOOH heterostructure electrocatalyst to enhance HMFOR [87]. DFT theoretical calculations and experimental characterization revealed that electron transfer occurred at the heterostructure surface (from CoOOH to CoP), enhancing its conductivity and adjusting the adsorption energy of HMF. At 1.42 V vs. RHE potential, HMF oxidation with a concentration of 150 mM was achieved, with an HMF conversion of 98.3% and an FDCA yield and FE of 96.3%. Li and co-workers utilized a controlled pyrolysis strategy to construct a Y-Co-CoS_x@CN heterostructure [88]. The catalyst demonstrated excellent HMFOR performance at a low potential (1.29 V vs. RHE), achieving full HMF conversion with an FDCA yield of 96% and FE of 93.5%. DFT calculations indicated that the construction of the Co-CoS_x heterostructure induced asymmetric arrangement of d-orbital electrons in the spin channel, resulting in strong spin polarization. This pushed the electronic states towards the Fermi level, enhancing the adsorption capability of the reactants/intermediates. The effective d-p coupling between the catalyst and reactants/intermediates accounted for the lower activation energy in the rate-determining step, providing favorable energy input for the overall HMFOR process. Similarly, Li and co-workers developed a CoP/Ni₂P-NiCoP@NC heterostructure material, which exhibited strong electronic coupling between the abundant heterogeneous interfaces (i.e., CoP, Ni₂P, and NiCoP) [89]. Further DFT theoretical calculations revealed that the heterogeneous interfaces in CoP/Ni₂P-NiCoP@NC could adjust the d-band center of Co and Ni close to the Fermi level, thereby enhancing the electron interaction on the reaction

interface and minimizing the energy barrier of the HMFOR rate-determining step. The optimized CoP/Ni₂P -NiCoP@NC-600 catalyst showed excellent HMF oxidation activity with an FDCA yield of 98.1% and FE of 97.6% at 1.32 V vs. RHE low potential. Du and co-workers developed Ni(OH)₂-NiOOH/NiFeP heterostructures, which exhibited outstanding catalytic activity for HMFOR with an FDCA yield exceeding 99% and an FE exceeding 94% [90]. More notably, the dynamic surface transformation process of the heterostructure catalyst for HMFOR was studied. It was found that during the HMFOR anodic process, NiFeP inevitably oxidized and generated Ni(OH)₂. With an increase in electrode potential, Ni(OH)₂ was further oxidized to form NiOOH, which acted as the true active site for HMFOR. This process was likely a chemical oxidation process rather than an electrochemical oxidation. After HMFOR, NiOOH was chemically reduced back to Ni(OH)₂, and the applied anodic potential continued to oxidize Ni(OH)₂ to NiOOH, cyclically driving the continuous progression of HMFOR. Similarly, Qiu and co-workers developed an Ni₃N–NiMoN/CC heterostructure catalyst and achieved complete HMF conversion with an FDCA yield of 98% and an FE close to 100% at 1.40 V vs. RHE potential [91]. Mu and co-workers developed a P and O co-doped Ni₂P–Ni₁₂P₅ heterostructure catalyst (t-Ni-P@POC), achieving complete HMF conversion with an FDCA yield of 99.9% and an FE of 99.7% at 1.42 V vs. RHE potential [92].

Recently, Wang and co-workers synthesized Co-Ni_xP@C heterostructure catalysts on Ni-Co metal foam. The results showed that CoNi_xP@C had a layered structure with a nanowire-like network, providing sufficient exposed active sites to enhance HMF molecule adsorption and activation, as well as optimizing the free energy of H⁺ adsorption [93]. The thin outer layer of graphite-like carbon enhanced the conductivity and stability of the catalyst. Furthermore, the cobalt-doped Ni₁₂P₅/Ni₃P heterostructures exhibited evident interface lattice mismatch and abundant defects, which effectively regulated the electronic structure and active sites. The catalyst achieved an HMF conversion and FDCA yield both close to 100%, with an FE of 99.7% at 1.38 V vs. RHE potential. Wang and co-workers constructed Co₃O₄/CeO₂ heterostructures on nickel foam [94]. The synthesized NF@Co₃O₄/CeO₂ heterostructure catalyst achieved 98% HMF conversion with an FDCA yield of 94.5% and FE of 97.5% at 1.40 V vs. RHE potential. The results indicated that the establishment of heterostructure interfaces effectively regulated intermediate adsorption and promoted electron transfer (from Co₃O₄ to CeO₂), significantly reducing the activation energy of FFCA dehydrogenation and facilitated the further oxidation of FFCA to FDCA, and thereby improving the performance of HMFOR. Similarly, Wang and co-workers synthesized NF/Co₄N@CeO₂ heterostructures supported by nickel foam [95]. The results demonstrated that CeO₂, acting as an “electron pump”, facilitated electron transfer from Co₄N to CeO₂, leading to charge redistribution at the heterostructure interface. NF/Co₄N@CeO₂ exhibited excellent HMFOR activity in alkaline media, with an HMF conversion of 91.1%, FDCA yield of 93.6%, and FE of 84.5% at a potential of 1.425 V vs. RHE. Li and co-workers developed Cu₂P₇-CoP heterostructure nanosheets as electrocatalysts for HMFOR, which could achieve the complete conversion of 10 mM HMF at a potential of 1.43 V vs. RHE [96]. The FDCA yield was 98.8% and the FE was 98%. Mou and co-workers reported a successful synthesis of a series of metal sulfide/metal phosphide (MS_x/MP_y, M = Co, Fe, Ni, etc.) heterojunctions using a sequential electrodeposition interface engineering strategy. Among them, the NiS_x/Ni₂P heterojunction had the optimal HMFOR catalytic activity [97]. At a potential of 1.425 V vs. RHE, HMF was almost completely converted with an FDCA yield of 98.5% and FE of 95.1%. The results showed that enrichment in heterogeneous interfaces promoted electron transfer between NiS_x and Ni₂P, synergistically increasing the oxidation valence state of Ni and further enhancing the catalytic performance of HMFOR. Ye and co-workers synthesized an NiFeP@NiFe(OH)_x heterojunction catalyst by using a two-step electrodeposition method [98]. As a nuclear, NiFeP has been found to have higher conductivity and promote charge transfer. On the other hand, the outer layer of NiFe(OH)_x could effectively protect the NiFeP core from further oxidation and reconstruction. At a potential of 1.45 V vs. RHE, an FE of 94.42% could

be achieved. Similarly, Zhang and co-workers developed a simple one-pot hydrothermal method and a two-step sequential deposition process to prepare a Ni(OH)₂-Cu₂O/NF-6 heterojunction catalyst [99]. At a potential of 1.424 V vs. RHE, the conversion of 50 mM HMF was achieved, with an FDCA yield of 91% and FE of 98%. Zhang and co-workers reported a Ni/Ni_{0.2}Mo_{0.8}N/NF heterojunction deposited on nickel foam and found that NiOOH was the real active site [100]. At a potential of 1.423 V vs. RHE, this heterojunction could achieve the nearly complete conversion of HMF, with an FDCA yield of 98.5% and FE close to 100%. Chen and co-workers constructed porous Ni-VN heterostructure nanosheets (Ni-VN/NF) on nickel foam [101]. Thanks to the surface reconstruction of the Ni-VN heterostructures in the oxidation process, the derived NiOOH-VN/NF had good HMFOR catalytic performance. At a lower oxidation potential (1.402 V vs. RHE), a higher HMF conversion rate (>99%) was achieved, with an FDCA yield of 99%, an FE >98%, and good cycling stability. The results indicated that the high activity of Ni-VN/NF mainly came from the local electron redistribution at the heterojunction interface, which accelerated charge transfer by adjusting the d-band center and optimized the adsorption of reactants/intermediates.

Recently, Yin and co-workers synthesized NiCo₂@MoO₂/NF heterojunction materials via a simple hydrothermal and calcination method [102]. The experimental and DFT theoretical calculation results showed that introducing MoO₂ on the surface of NiCo₂ could regulate the electronic structure of NiCo₂@MoO₂/NF, optimized the adsorption behavior of HMFOR intermediates, and promoted the dehydrogenation of key intermediate HMFCa to FFCA by weakening the C-H/O-H bond (Figure 11). The deuterium isotope kinetic effects and proton transfer experiments indicated that the interaction between MoO₂ and NiCo₂ promoted proton transfer and the cleavage of C-H/O-H bonds in the HMFOR process. In addition, the catalyst exhibited excellent HMFOR catalytic performance, achieving the almost complete conversion of HMF at a potential of 1.40 V vs. RHE. The FDCA yield was 99.6%, and the FE was close to 99.4%. Lee and co-workers compared and analyzed the different reactivities of NiOOH and Cu(OH)₂ in the electrochemical oxidation of alcohols and aldehydes on the furan ring and utilized their synergistic effect to improve the catalytic performance of HMFOR [103]. The results showed that the oxidation of alcohol in HMF was initiated by NiOOH, and Cu(OH)₂ could quickly convert the remaining aldehydes into carboxylic acids at the NiOOH/Cu(OH)₂ interface. Compared with individual NiOOH and Cu(OH)₂ electrodes, the NiOOH-Cu(OH)₂ mixed electrode had a higher catalytic activity and faster conversion rate. At a potential of 1.40 V vs. RHE, NiOOH-Cu(OH)₂ could achieve the almost complete conversion of HMF, with an FDCA yield of 98.3% and FE of 98.3%.

3.2.4. Other Catalysts

Table 5 summarizes recent advances in the electrocatalytic oxidation of HMF to synthesize FDCA using other catalysts, such as MOFs, COFs, and non-metal catalysts.

MOFs

Metal-organic frameworks (MOFs) have received widespread attention in the fields of gas separation, adsorption, and catalysis due to their definite structure and excellent structural performance [104,105]. Although there have been many reports on the use of MOF-based catalysts to catalyze the conversion of biomass into value-added products such as biofuels, fine chemicals, and functional materials, there are still fewer reports on the production of renewable plastic-related materials and precursors, especially in the applications of HMFOR, which are rarely reported [106,107].

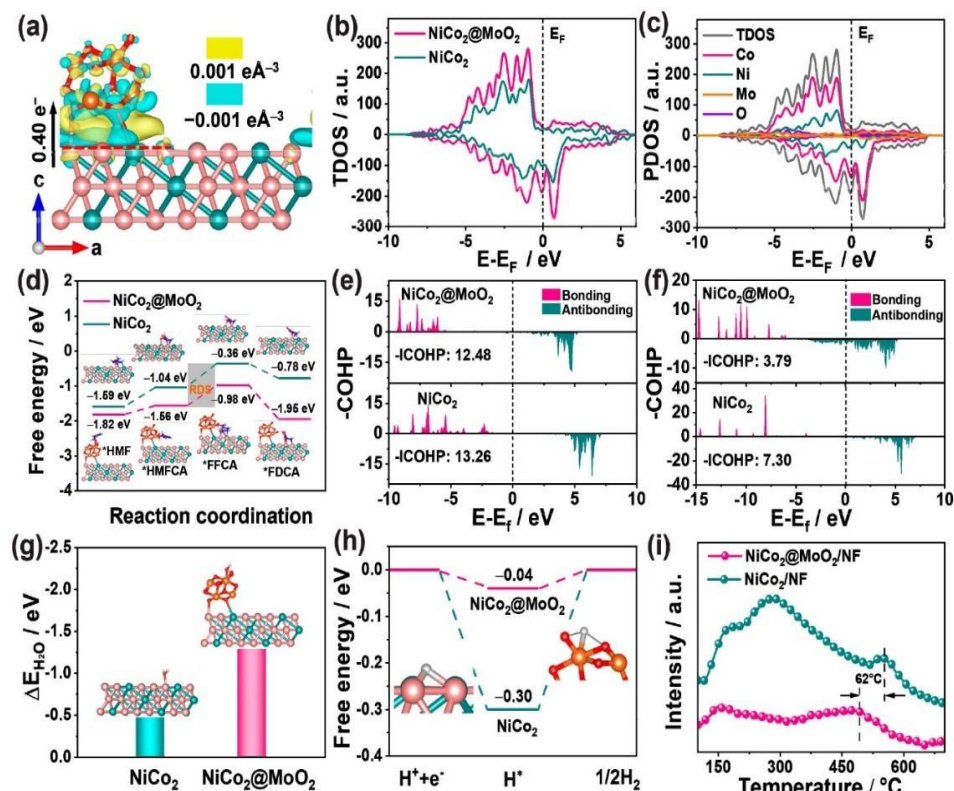


Figure 11. (a) Electron density difference of NiCo₂@MoO₂; (b) TDOS of NiCo₂ and NiCo₂@MoO₂; (c) PDOS of NiCo₂@MoO₂; (d) free-energy profiles of HMFOR on NiCo₂ and NiCo₂@MoO₂; –COHP of the (e) C–H and (f) O–H bonds of HMFO on NiCo₂ and NiCo₂@MoO₂; (g) H₂O and (h) H⁺ adsorption energy on NiCo₂ and NiCo₂@MoO₂; (i) TPD spectra of NiCo₂/NF and NiCo₂@MoO₂ under an H₂ atmosphere. Reproduced from Ref. [102]. Copyright 2023, with permission from American Chemical Society.

Table 5. HMFOR over other catalysts ^a.

Type	Catalyst	HMF (mM)	Potential (V vs. RHE)	HMF Conversion (%)	FDCA Yield (%)	FE (%)	Ref.
MOFs	NiCoBDC-NF	10	1.55	-	99 ^b	78.8 ^b	[108]
	Co(OH) ₂ @ZIF-67	10	1.42	90.9	81.8	83.6	[109]
	CoNiFe-MOFs/NF	10	1.40	100	99.76	100	[110]
	Rbf-Ni-MOF	10	0.8	-	-	95	[111]
	Co-CAT	10	1.42	-	99.3	97.6	[112]
	Ni-CAT	10	1.42	-	98.7	86.8	[112]
	CF-Ni-MOF/Ag	10	1.623	~100	-	98.6	[113]
	CF-CuO/Ni-BTC MOF	10	0.55	~100	99.9	91	[114]
COFs	NiCoFeS-MOF	50	1.39	100	99	99	[115]
	TpBpy-Ni@FTO	0.5	1.55	96 ^c	58 ^c	-	[116]
non-metal	B–N codoped porous carbons (BNC-2)	5	1.90	71 ^b	57 ^b	-	[117]

^a The electrocatalytic oxidation of HMF was tested in 1.0 M KOH. ^b 0.1 M KOH. ^c 0.1 M LiClO₄.

In 2020, Li and co-workers synthesized a series of metal-doped (Co, Fe, and Mn) two-dimensional Ni-MOFs through the solvothermal method, and MOFs were used as electrocatalysts for HMFOR for the first time. It was found that co-doped NiCoBDC-NF exhibited good activity, selectivity, and stability towards HMFOR [108]. In an electrolyte with a pH of 13, the FDCA yield was as high as 20.1 μmol cm⁻² h⁻¹ at a potential of 1.55 V vs. RHE, with a yield

of up to 99% and an FE of 78.8%. It could catalyze continuously for four cycles. The results indicated that the coupling effect between co-doped Ni and Co atoms optimized the electronic structure and made it easy to form high-valence Ni species in two-dimensional MOFs, which were considered active sites for aldehyde and alcohol oxidation. This work provided a reference and important basis for exploring the application of two-dimensional MOF electrocatalytic materials in HMFOR in the future. In 2021, Kongpathanich and co-workers prepared ultra-thin $\text{Co}(\text{OH})_2$ layers on ZIF-67 thin films by using electrochemical treatment [109]. The prepared composite film $\text{Co}(\text{OH})_2/\text{ZIF-67}$ served as an HMFOR electrocatalyst and exhibited excellent catalytic performance. At a potential of 1.42 V vs. RHE, the conversion of HMF was 90.9%, the yield of FDCA was 81.8%, and the FE was 83.6%. The results indicated that the porous structure in the MOFs promoted mass transfer and the ultra-thin $\text{Co}(\text{OH})_2$ layers were electrochemical active sites. Qi and co-workers developed a simple solvothermal synthesis method to prepare ternary (Co, Ni, and Fe) MOF nanoarrays CoNiFe MOFs/NF on Ni foam [110]. CoNiFe MOFs/NF had a compact array nanostructure of vertically grown nanosheets and had remarkable HMFOR performance. Under 1.4 V vs. RHE potential, the HMF conversion rate was 100%, the FDCA yield was up to 99.76%, and the FE was close to 100%. In addition, the catalyst also showed high stability, and the yield of FDCA remained basically above 96% over 15 consecutive cycles of HMFOR. The results indicated that the high activity of the catalyst was due to the synergistic effect among the unique two-dimensional microporous MOF structure, the in situ growth method, and the effective control of electronic structure by mixed metals.

In 2022, Karvembu and co-workers incorporated redox-active riboflavin (Rbf) into a Ni-MOF by using a green and convenient mechanochemical method [111]. The conductivity of the Rbf-doped Ni-MOF (Rbf-Ni-MOF) was four-fold higher than the original Ni-MOF. In addition, the Rbf-Ni-MOF could achieve efficient HMFOR to generate FDCA with an FE exceeding 95%. DFT analysis showed that the addition of Rbf changed the band structure of the Ni-MOF and induced a certain conductivity, which helped the Rbf-Ni-MOF exhibit enhanced electrocatalytic activity. Zhang and co-workers developed an electrocatalytic model system (M-CATs, M = Co, Ni, Cu, etc.) based on conductive MOFs, which had well-defined M-O_4 active sites and exhibited excellent catalytic activity for HMFOR [112]. For example, at a potential of 1.42 V vs. RHE, the Co-CAT catalyst could achieve an FDCA yield up to 99.3% and FE of 97.6%. When the Ni-CAT catalyst was used, the FDCA yield was 98.7% and the FE was 86.8%. Meanwhile, the infrared spectroscopy (IR) results found that HMFOR was caused by the generation of M^{III} and subsequent aldehyde adsorption of HMF. The adsorption of the reactant was the rate-limiting step of Co-CAT, while the rate-limiting step of Ni-CAT was intermediate desorption.

Recently, Fan and co-workers induced the interface activation of Ni-MOF/Ag through in situ electrochemical reconstruction strategy [113]. The activated CF-Ni-MOF/Ag (CF, Cu foam) showed good electrocatalytic performance for HMFOR. At 1.625 V vs. RHE potential, HMF was almost completely converted, and the FE was close to 98.6%. The results indicated that the synergistic effect of $\text{Ni}^{3+}/\text{Ag}^+$ was the main source of the high activity of CF-Ni-MOF/Ag, and the high-valence $\text{Ni}^{3+}/\text{Ag}^+$ generated by oxidation activation was the main active site. Using a similar electrochemical reconstruction strategy, Fan and co-workers reconstructed CuO/Ni-MOF to synthesize a CF-CuO/Ni-BTC MOF electrocatalyst and applied it to HMFOR (Figure 12) [114]. The results indicated that $\text{CuOOH}/\text{NiOOH}$ was the main active site for HMFOR, which simultaneously exhibited excellent self-healing ability, and contributed to the regeneration and long-term stability of the catalyst. In addition, a dual-chamber electrocatalytic system combining HMFOR with 4-nitrophenol hydrogenation was established. The results showed that under the condition of 0.55 V vs. Ag/AgCl (3.0 h), the current density of the entire reaction reached $47.6 \text{ mA}/\text{cm}^2$, and the corresponding conversion and FE were both close to 100%. Recently, Qi and co-workers employed a simple solvothermal method to embed Ni/Co/Fe sulfide nanoclusters into MOF nanoarrays [115]. The prepared NiCoFeS-MOF catalyst had a staggered structure, and the combination of metal sulfide nanoclusters with two-dimensional MOF nanoarrays greatly expanded the electrochemical active surface area, increased the number of active catalytic sites, and improved electron transfer. HMF achieved complete conversion at 1.39 V vs. RHE with an FDCA yield and FE that both reached 99%.

COFs

Covalent organic frameworks (COFs) are novel organic porous polymer materials formed by covalent bonds (such as B-O, C-N, or C-C) between organic monomers in the two-dimensional or three-dimensional direction. In recent years, due to its advantages such as low skeleton density, large specific surface area, uniform pore size distribution, high porosity, high crystallinity, high stability, and designable structural units, it has become a research frontier and hotspot in the field of materials science. It has shown good application prospects in gas adsorption and separation, catalysis, optoelectronics, drug delivery, chemical sensing, energy storage, and chromatographic separation [118,119].

In 2020, Cai and co-workers prepared a nickel (II)-modified covalent organic framework (COF) membrane TpBpy-Ni@FTO and applied it to HMFOR [116]. The results indicated that the conversion of HMF was as high as 96% while the selectivity of FDCA was poor with an FDCA yield of 58%. This was the first example of COFs being applied to HMFOR, but the catalytic performance was still not ideal. This work provided a certain reference and optimization basis for biomass electrocatalysis with a COF structure in the future.

Non-Metal Catalysts

So far, developing non-metal catalysts for HMFOR still remains a huge challenge. In 2019, Qin and co-workers constructed N and B co-doped porous carbon BNC-2 with enrich point defects and polar pore wall structures [117]. This was the first non-metal electrocatalyst used for HMFOR. The results showed that the HMF conversion was 71% and the FDCA yield was 57% at a reaction potential of 1.9 V and a reaction time of 6 h. Although its catalytic performance was not as good as that of metal-based catalysts, it also provided valuable experience for the development and design of non-metal material electrocatalysts.

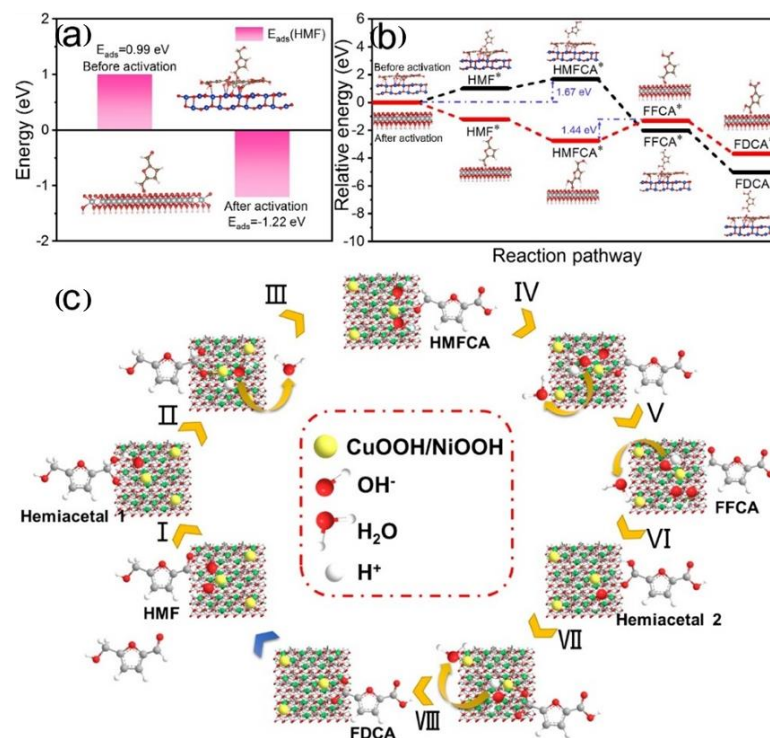


Figure 12. The adsorption energy of CF-CuO/Ni-BTC MOF for HMF (a). Standard free-energy diagrams of HMF → FDCA on the surfaces of CF-CuO/Ni-BTC MOF (b). The electrocatalytic mechanism of activated CF-CuO/Ni-BTC MOF for HMF → FDCA (c). Reproduced from Ref. [114]. Copyright 2023, with permission from Elsevier.

4. Conclusions and Prospects

Biomass-derived HMF is an important building block and one of the most versatile bio-based platform molecules. Its oxidation product FDCA is regarded as a substitute for the petroleum derivative terephthalic acid (TPA), and the bio-based plastic polyethylene-2,5-furandicarboxylate (PEF) polymerized with FDCA monomer is expected to replace the petroleum-based plastic polyethylene terephthalate (PET) in industry. Therefore, based on the huge economic and sustainable benefits, the preparation of FDCA by the electrochemical oxidation of HMF has received extensive attention in recent years.

In this review, we summarized the latest progress of heterogeneous catalysts in the synthesis of FDCA by HMFOR. First, we introduced the reaction path of HMFOR and the calculation method of electrocatalytic activity. Second, in order to gain a deeper understanding of the reaction, we summarize the currently accepted reaction mechanisms (i.e., direct oxidation and indirect oxidation), which can also provide theoretical guidance for understanding the electrochemical oxidation of other small organic molecules containing alcohols or aldehydes. In addition, we summarized and compared the research progress of various heterogeneous catalysts applied to the electrochemical oxidation of HMF to FDCA in chronological order, focusing on the research progress of non-noble metal catalysts, such as (1) non-noble metal phosphides, sulfides, borides, and nitrides; (2) non-noble metal hydroxides and oxides; (3) heterojunctions; (4) and other catalysts such as MOFs, COFs, and non-metallic catalysts.

Despite the rapid development of the HMF electrochemical oxidation synthesis of FDCA with reported high HMF conversion rates and high FDCA yields and FEs, there still remain scientific challenges and technological gaps. It is worth noting that most laboratory-scale investigations fall short of meeting the demands of industrial production, often being limited to relatively low current densities and mM-level HMF additions. Therefore, in order to further enhance catalytic activity, reduce costs, and promote the practical application of HMF electro-oxidation technology, future research should focus on the following aspects:

1. Strengthening the understanding of reaction mechanisms, pathways, and the true catalytic active sites through the utilization of in situ characterization techniques.
2. Combining experimental studies with machine-learning algorithm tools to develop and design more catalyst-performance-based descriptors, which can facilitate the development of more efficient catalysts.
3. The development of large-scale electrocatalysts with high stability and activity under high current densities ($\geq 500 \text{ mA cm}^{-2}$) will be a crucial area of research in the future.
4. There is a need to develop efficient reactors suitable for electrochemical industrial production systems, as well as cost-effective separation and purification techniques.

Author Contributions: Z.M.: writing—original draft; writing—review & editing; supervision; funding acquisition. L.W.: writing—original draft. G.L.: writing—original draft. T.S.: writing—review & editing; supervision. All authors have read and agreed to the published version of the manuscript.

Funding: This research was funded by the High-level Talent Research Support Program of Shenyang Ligong University (No. 1010147001104). The National Natural Science Foundation of China (No. 22002178) are gratefully acknowledged.

Data Availability Statement: Data will be made available on request.

Conflicts of Interest: The authors declare that they have no known competing financial interests or personal relationships that could have appeared to influence the work reported in this paper.

References

1. Su, T.; Zhao, D.; Wang, Y.; Lü, H.; Varma, R.S.; Len, C. Innovative Protocols in the Catalytic Oxidation of 5-Hydroxymethylfurfural. *ChemSusChem* **2021**, *14*, 266–280. [[CrossRef](#)] [[PubMed](#)]
2. Yang, Y.; Mu, T. Electrochemical oxidation of biomass derived 5-hydroxymethylfurfural (HMF): Pathway, mechanism, catalysts and coupling reactions. *Green Chem.* **2021**, *23*, 4228–4254. [[CrossRef](#)]

3. Zhao, Y.; Cai, M.; Xian, J.; Sun, Y.; Li, G. Recent advances in the electrocatalytic synthesis of 2,5-furandicarboxylic acid from 5-(hydroxymethyl)furfural. *J. Mater. Chem. A* **2021**, *9*, 20164–20183. [[CrossRef](#)]
4. Guo, M.; Lu, X.; Xiong, J.; Zhang, R.; Li, X.; Qiao, Y.; Ji, N.; Yu, Z. Alloy-Driven Efficient Electrocatalytic Oxidation of Biomass-Derived 5-Hydroxymethylfurfural towards 2,5-Furandicarboxylic Acid: A Review. *ChemSusChem* **2022**, *15*, e202201074. [[CrossRef](#)]
5. Guo, L.; Zhang, X.; Gan, L.; Pan, L.; Shi, C.; Huang, Z.-F.; Zhang, X.; Zou, J.-J. Advances in Selective Electrochemical Oxidation of 5-Hydroxymethylfurfural to Produce High-Value Chemicals. *Adv. Sci.* **2023**, *10*, 2205540. [[CrossRef](#)]
6. Jing, Y.; Guo, Y.; Xia, Q.; Liu, X.; Wang, Y. Catalytic Production of Value-Added Chemicals and Liquid Fuels from Lignocellulosic Biomass. *Chem* **2019**, *5*, 2520–2546. [[CrossRef](#)]
7. Lin, Z.; Chen, X.; Lu, L.; Yao, X.; Zhai, C.; Tao, H. Recent advances in electrocatalytic oxidation of 5-hydroxymethylfurfural to 2,5-furandicarboxylic acid: Mechanism, catalyst, coupling system. *Nanotechnol. Rev.* **2023**, *12*, 20220518. [[CrossRef](#)]
8. Ge, R.; Li, J.; Duan, H. Recent advances in non-noble electrocatalysts for oxidative valorization of biomass derivatives. *Sci. China Mater.* **2022**, *65*, 3273–3301. [[CrossRef](#)]
9. Totaro, G.; Sisti, L.; Marchese, P.; Colonna, M.; Romano, A.; Gioia, C.; Vannini, M.; Celli, A. Current Advances in the Sustainable Conversion of 5-Hydroxymethylfurfural into 2,5-Furandicarboxylic Acid. *ChemSusChem* **2022**, *15*, e202200501. [[CrossRef](#)]
10. Jiang, X.; Li, W.; Liu, Y.; Zhao, L.; Chen, Z.; Zhang, L.; Zhang, Y.; Yun, S. Electrocatalytic oxidation of 5-hydroxymethylfurfural for sustainable 2,5-furandicarboxylic acid production—From mechanism to catalysts design. *SusMat* **2023**, *3*, 21–43. [[CrossRef](#)]
11. Meng, Y.; Yang, S.; Li, H. Electro- and Photocatalytic Oxidative Upgrading of Bio-based 5-Hydroxymethylfurfural. *ChemSusChem* **2022**, *15*, e202102581. [[CrossRef](#)]
12. German, D.; Pakrieva, E.; Kolobova, E.; Carabineiro, S.A.C.; Stucchi, M.; Villa, A.; Prati, L.; Bogdanchikova, N.; Cortés Corberán, V.; Pestryakov, A. Oxidation of 5-Hydroxymethylfurfural on Supported Ag, Au, Pd and Bimetallic Pd-Au Catalysts: Effect of the Support. *Catalysts* **2021**, *11*, 115. [[CrossRef](#)]
13. Chen, W.; Xie, C.; Wang, Y.; Zou, Y.; Dong, C.-L.; Huang, Y.-C.; Xiao, Z.; Wei, Z.; Du, S.; Chen, C.; et al. Activity Origins and Design Principles of Nickel-Based Catalysts for Nucleophile Electrooxidation. *Chem* **2020**, *6*, 2974–2993. [[CrossRef](#)]
14. Ma, Z.; Liu, S.; Tang, N.; Song, T.; Motokura, K.; Shen, Z.; Yang, Y. Coexistence of Fe Nanoclusters Boosting Fe Single Atoms to Generate Singlet Oxygen for Efficient Aerobic Oxidation of Primary Amines to Imines. *ACS Catal.* **2022**, *12*, 5595–5604. [[CrossRef](#)]
15. Ma, Z.; Song, T.; Yuan, Y.; Yang, Y. Synergistic catalysis on Fe–Nx sites and Fe nanoparticles for efficient synthesis of quinolines and quinazolinones via oxidative coupling of amines and aldehydes. *Chem. Sci.* **2019**, *10*, 10283–10289. [[CrossRef](#)]
16. Vuyyuru, K.R.; Strasser, P. Oxidation of biomass derived 5-hydroxymethylfurfural using heterogeneous and electrochemical catalysis. *Catal. Today* **2012**, *195*, 144–154. [[CrossRef](#)]
17. Chadderton, D.J.; Xin, L.; Qi, J.; Qiu, Y.; Krishna, P.; More, K.L.; Li, W. Electrocatalytic oxidation of 5-hydroxymethylfurfural to 2,5-furandicarboxylic acid on supported Au and Pd bimetallic nanoparticles. *Green Chem.* **2014**, *16*, 3778–3786. [[CrossRef](#)]
18. Xu, G.-R.; Batmunkh, M.; Donne, S.; Jin, H.; Jiang, J.-X.; Chen, Y.; Ma, T. Ruthenium(iii) polyethyleneimine complexes for bifunctional ammonia production and biomass upgrading. *J. Mater. Chem. A* **2019**, *7*, 25433–25440. [[CrossRef](#)]
19. Park, M.; Gu, M.; Kim, B.-S. Tailorable Electrocatalytic 5-Hydroxymethylfurfural Oxidation and H₂ Production: Architecture–Performance Relationship in Bifunctional Multilayer Electrodes. *ACS Nano* **2020**, *14*, 6812–6822. [[CrossRef](#)] [[PubMed](#)]
20. Liu, G.; Nie, T.; Song, Z.; Sun, X.; Shen, T.; Bai, S.; Zheng, L.; Song, Y.-F. Pd Loaded NiCo Hydroxides for Biomass Electrooxidation: Understanding the Synergistic Effect of Proton Deintercalation and Adsorption Kinetics. *Angew. Chem. Int. Ed.* **2023**, *62*, e202311696. [[CrossRef](#)] [[PubMed](#)]
21. Lu, Y.; Liu, T.; Dong, C.-L.; Huang, Y.-C.; Li, Y.; Chen, J.; Zou, Y.; Wang, S. Tuning the Selective Adsorption Site of Biomass on Co₃O₄ by Ir Single Atoms for Electrosynthesis. *Adv. Mater.* **2021**, *33*, 2007056. [[CrossRef](#)] [[PubMed](#)]
22. Gu, W.; Pei, A.; Zhang, S.; Jiang, F.; Jia, Y.; Qin, Q.; Du, R.; Li, Z.; Liu, R.; Qiu, Y.; et al. Atomic-Interface Effect of Single-Atom Ru/CoOx for Selective Electrooxidation of 5-Hydroxymethylfurfural. *ACS Appl. Mater. Interfaces* **2023**, *15*, 28036–28043. [[CrossRef](#)] [[PubMed](#)]
23. Zeng, L.; Chen, Y.; Sun, M.; Huang, Q.; Sun, K.; Ma, J.; Li, J.; Tan, H.; Li, M.; Pan, Y.; et al. Cooperative Rh-O5/Ni(Fe) Site for Efficient Biomass Upgrading Coupled with H₂ Production. *J. Am. Chem. Soc.* **2023**, *145*, 17577–17587. [[CrossRef](#)] [[PubMed](#)]
24. Xu, H.; Xin, G.; Hu, W.; Zhang, Z.; Si, C.; Chen, J.; Lu, L.; Peng, Y.; Li, X. Single-atoms Ru/NiFe layered double hydroxide electrocatalyst: Efficient for oxidation of 5-hydroxymethylfurfural and oxygen evolution reaction. *Appl. Catal. B* **2023**, *339*, 123157. [[CrossRef](#)]
25. Han, X.; Zhang, T.; Wang, X.; Zhang, Z.; Li, Y.; Qin, Y.; Wang, B.; Han, A.; Liu, J. Hollow mesoporous atomically dispersed metal-nitrogen-carbon catalysts with enhanced diffusion for catalysis involving larger molecules. *Nat. Commun.* **2022**, *13*, 2900. [[CrossRef](#)] [[PubMed](#)]
26. Sun, Q.; Jia, C.; Zhao, Y.; Zhao, C. Single atom-based catalysts for electrochemical CO₂ reduction. *Chin. J. Catal.* **2022**, *43*, 1547–1597. [[CrossRef](#)]
27. Kim, J.; Yoo, J.M.; Lee, H.S.; Sung, Y.-E.; Hyeon, T. Single-atom M–N–C catalysts for oxygen reduction electrocatalysis. *Trends Chem.* **2021**, *3*, 779–794. [[CrossRef](#)]
28. Shang, Y.; Xu, X.; Gao, B.; Wang, S.; Duan, X. Single-atom catalysis in advanced oxidation processes for environmental remediation. *Chem. Soc. Rev.* **2021**, *50*, 5281–5322. [[CrossRef](#)]
29. Yuan, L.-J.; Sui, X.-L.; Liu, C.; Zhuo, Y.-L.; Li, Q.; Pan, H.; Wang, Z.-B. Electrocatalysis Mechanism and Structure–Activity Relationship of Atomically Dispersed Metal-Nitrogen-Carbon Catalysts for Electrocatalytic Reactions. *Small Methods* **2023**, *7*, 2201524. [[CrossRef](#)]

30. Zhang, L.; Meng, Q.; Zheng, R.; Wang, L.; Xing, W.; Cai, W.; Xiao, M. Microenvironment regulation of M-N-C single-atom catalysts towards oxygen reduction reaction. *Nano Res.* **2023**, *16*, 4468–4487. [[CrossRef](#)]
31. Yang, G.; Jiao, Y.; Yan, H.; Tian, C.; Fu, H. Electronic Structure Modulation of Non-Noble-Metal-Based Catalysts for Biomass Electrooxidation Reactions. *Small Struct.* **2021**, *2*, 2100095. [[CrossRef](#)]
32. Song, Y.; Xie, W.; Song, Y.; Li, H.; Li, S.; Jiang, S.; Lee, J.Y.; Shao, M. Bifunctional integrated electrode for high-efficient hydrogen production coupled with 5-hydroxymethylfurfural oxidation. *Appl. Catal. B* **2022**, *312*, 121400. [[CrossRef](#)]
33. Jiang, N.; You, B.; Boonstra, R.; Terrero Rodriguez, I.M.; Sun, Y. Integrating Electrocatalytic 5-Hydroxymethylfurfural Oxidation and Hydrogen Production via Co-P-Derived Electrocatalysts. *ACS Energy Lett.* **2016**, *1*, 386–390. [[CrossRef](#)]
34. You, B.; Jiang, N.; Liu, X.; Sun, Y. Simultaneous H₂ Generation and Biomass Upgrading in Water by an Efficient Noble-Metal-Free Bifunctional Electrocatalyst. *Angew. Chem. Int. Ed.* **2016**, *55*, 9913–9917. [[CrossRef](#)] [[PubMed](#)]
35. Li, M.; Chen, L.; Ye, S.; Fan, G.; Yang, L.; Zhang, X.; Li, F. Dispersive non-noble metal phosphide embedded in alumina arrays derived from layered double hydroxide precursor toward efficient oxygen evolution reaction and biomass upgrading. *J. Mater. Chem. A* **2019**, *7*, 13695–13704. [[CrossRef](#)]
36. Liu, S.; Yuan, X.; Huang, X.; Huang, Y.; Sun, C.; Qian, K.; Zhang, W. Nickel-phytic acid hybrid for highly efficient electrocatalytic upgrading of HMF. *Front. Chem.* **2023**, *11*, 1199921. [[CrossRef](#)] [[PubMed](#)]
37. Dasgupta, B.; Hausmann, J.N.; Beltrán-Suito, R.; Kalra, S.; Laun, K.; Zebger, I.; Driess, M.; Menezes, P.W. A Facile Molecular Approach to Amorphous Nickel Phosphides and Their Reconstruction to Crystalline Potassium-Intercalated γ -NiOOH_x Enabling High-Performance Electrocatalytic Water Oxidation and Selective Oxidation of 5-Hydroxymethylfurfural. *Small* **2023**, *19*, 2301258. [[CrossRef](#)] [[PubMed](#)]
38. Lin, R.; Salehi, M.; Guo, J.; Seifitokaldani, A. High oxidation state enabled by plated Ni-P achieves superior electrocatalytic performance for 5-hydroxymethylfurfural oxidation reaction. *iScience* **2022**, *25*, 104744. [[CrossRef](#)] [[PubMed](#)]
39. Gong, W.; Li, J.; Ma, J.; Liu, D.; Long, R.; Xiong, Y. Highly efficient electrocatalytic biomass valorization over a perovskite-derived nickel phosphide catalyst. *Nanoscale Horiz.* **2023**, *8*, 69–74. [[CrossRef](#)]
40. Bi, J.; Ying, H.; Xu, H.; Zhao, X.; Du, X.; Hao, J.; Li, Z. Phosphorus vacancy-engineered Ce-doped CoP nanosheets for the electrocatalytic oxidation of 5-hydroxymethylfurfural. *Chem. Commun.* **2022**, *58*, 7817–7820. [[CrossRef](#)]
41. Xie, S.; Fu, H.; Chen, L.; Li, Y.; Shen, K. Carbon-based nanoarrays embedded with Ce-doped ultrasmall Co₂P nanoparticles enable efficient electrooxidation of 5-hydroxymethylfurfural coupled with hydrogen production. *Sci. China Chem.* **2023**, *66*, 2141–2152. [[CrossRef](#)]
42. Xu, H.; Bi, J.; Sang, T.; Wang, W.; Hao, J.; Li, Z. Mn-doped Ni₂P: Nanocrystal-decorated amorphous nanosheets for efficient electrooxidation of 5-hydroxymethylfurfural. *Chem. Commun.* **2023**, *59*, 8440–8443. [[CrossRef](#)]
43. Zhang, H.; Qi, G.; Liu, W.; Zhang, S.; Liu, Q.; Luo, J.; Liu, X. Bimetallic phosphoselenide nanosheets as bifunctional catalysts for 5-hydroxymethylfurfural oxidation and hydrogen evolution. *Inorg. Chem. Front.* **2023**, *10*, 2423–2429. [[CrossRef](#)]
44. Wang, H.; Niu, C.; Liu, W.; Tao, S. d-Electron tuned CoMoP for enhance 5-hydroxymethylfurfural oxidation and HER. *Appl. Catal. B* **2024**, *340*, 123249. [[CrossRef](#)]
45. You, B.; Liu, X.; Jiang, N.; Sun, Y. A General Strategy for Decoupled Hydrogen Production from Water Splitting by Integrating Oxidative Biomass Valorization. *J. Am. Chem. Soc.* **2016**, *138*, 13639–13646. [[CrossRef](#)]
46. Wang, W.; Kong, F.; Zhang, Z.; Yang, L.; Wang, M. Sulfidation of nickel foam with enhanced electrocatalytic oxidation of 5-hydroxymethylfurfural to 2,5-furandicarboxylic acid. *Dalton Trans.* **2021**, *50*, 10922–10927. [[CrossRef](#)]
47. Kong, F.; Wang, M. Preparation of Sulfur-Modulated Nickel/Carbon Composites from Lignosulfonate for the Electrocatalytic Oxidation of 5-Hydroxymethylfurfural to 2,5-Furandicarboxylic Acid. *ACS Appl. Energy Mater.* **2021**, *4*, 1182–1188. [[CrossRef](#)]
48. Zhao, Z.; Guo, T.; Luo, X.; Qin, X.; Zheng, L.; Yu, L.; Lv, Z.; Ma, D.; Zheng, H. Bimetallic sites and coordination effects: Electronic structure engineering of NiCo-based sulfide for 5-hydroxymethylfurfural electrooxidation. *Catal. Sci. Technol.* **2022**, *12*, 3817–3825. [[CrossRef](#)]
49. Sun, Y.; Wang, J.; Qi, Y.; Li, W.; Wang, C. Efficient Electrooxidation of 5-Hydroxymethylfurfural Using Co-Doped Ni₃S₂ Catalyst: Promising for H₂ Production under Industrial-Level Current Density. *Adv. Sci.* **2022**, *9*, 2200957. [[CrossRef](#)]
50. Guo, C.; Huo, Y.; Zhang, Q.; Wan, K.; Yang, G.; Liu, Z.; Peng, F. MOF Material-Derived Bimetallic Sulfide Co_xNi_yS for Electrocatalytic Oxidation of 5-Hydroxymethylfurfural. *Nanomaterials* **2023**, *13*, 2318. [[CrossRef](#)]
51. Li, S.; Wang, S.; Wang, Y.; He, J.; Li, K.; Xu, Y.; Wang, M.; Zhao, S.; Li, X.; Zhong, X.; et al. Doped Mn Enhanced NiS Electrooxidation Performance of HMF into FDCA at Industrial-Level Current Density. *Adv. Funct. Mater.* **2023**, *33*, 2214488. [[CrossRef](#)]
52. Xu, P.; Bao, Z.; Zhao, Y.; Zheng, L.; Lv, Z.; Shi, X.; Wang, H.-E.; Fang, X.; Zheng, H. Anionic Regulation and Heteroatom Doping of Ni-Based Electrocatalysts to Boost Biomass Valorization Coupled with Hydrogen Production. *Adv. Energy Mater.* **2024**, *14*, 2303557. [[CrossRef](#)]
53. Wang, S.; Yang, G.; Jiao, Y.; Liu, Y.; Tian, C.; Wu, A.; Yan, H. Tuning electronic structure of Ni₃S₂ with tungsten doping for high-performance electrooxidation of 5-hydroxymethylfurfural. *Sci. China Chem.* **2023**, *66*, 3636–3644. [[CrossRef](#)]
54. Barwe, S.; Weidner, J.; Cychy, S.; Morales, D.M.; Dieckhöfer, S.; Hiltrop, D.; Masa, J.; Muhler, M.; Schuhmann, W. Electrocatalytic Oxidation of 5-(Hydroxymethyl)furfural Using High-Surface-Area Nickel Boride. *Angew. Chem. Int. Ed.* **2018**, *57*, 11460–11464. [[CrossRef](#)] [[PubMed](#)]

55. Zhang, P.; Sheng, X.; Chen, X.; Fang, Z.; Jiang, J.; Wang, M.; Li, F.; Fan, L.; Ren, Y.; Zhang, B.; et al. Paired Electrocatalytic Oxygenation and Hydrogenation of Organic Substrates with Water as the Oxygen and Hydrogen Source. *Angew. Chem. Int. Ed.* **2019**, *58*, 9155–9159. [CrossRef] [PubMed]
56. Song, X.; Liu, X.; Wang, H.; Guo, Y.; Wang, Y. Improved Performance of Nickel Boride by Phosphorus Doping as an Efficient Electrocatalyst for the Oxidation of 5-Hydroxymethylfurfural to 2,5-Furandicarboxylic Acid. *Ind. Eng. Chem. Res.* **2020**, *59*, 17348–17356. [CrossRef]
57. Zhang, N.; Zou, Y.; Tao, L.; Chen, W.; Zhou, L.; Liu, Z.; Zhou, B.; Huang, G.; Lin, H.; Wang, S. Electrochemical Oxidation of 5-Hydroxymethylfurfural on Nickel Nitride/Carbon Nanosheets: Reaction Pathway Determined by In Situ Sum Frequency Generation Vibrational Spectroscopy. *Angew. Chem. Int. Ed.* **2019**, *58*, 15895–15903. [CrossRef]
58. Zhou, B.; Dong, C.-L.; Huang, Y.-C.; Zhang, N.; Wu, Y.; Lu, Y.; Yue, X.; Xiao, Z.; Zou, Y.; Wang, S. Activity origin and alkalinity effect of electrocatalytic biomass oxidation on nickel nitride. *J. Energy Chem.* **2021**, *61*, 179–185. [CrossRef]
59. Zhang, D.; Xing, M.; Mou, X.; Song, C.; Wang, D. Deep eutectic solvent induced ultrathin Co₄N/N-doped carbon nanosheets self-supporting electrode for boosting hydrogen evolution integrated with biomass electrooxidation. *Appl. Surf. Sci.* **2023**, *608*, 155283. [CrossRef]
60. Xiao, Y.; Shen, C.; Xiong, Z.; Ding, Y.; Liu, L.; Zhang, W.; Wu, Y.A. Electrocatalytic upgrading biomass approach to address oxidation of 5-(Hydroxymethyl)furfural using Mo₂B₂ MBene active surface. *Mater. Today Phys.* **2023**, *35*, 101122. [CrossRef]
61. Chen, H.; Lv, X.; Li, S.; Hu, Y.; Li, F. Preparation and performance of phosphorus-doped NiCo LDH for oxygen evolution reaction. *J. Shenyang Ligong Univ.* **2023**, *42*, 61–67. Available online: https://kns.cnki.net/kcms2/article/abstract?v=BS8_DD2Uwa4Z0uIE8AWWa6Q4dwaalSsTyWB3VbTU5czEMU2uVPuqKV8ioBRzgzS4E4m5y5F2-oByJPYYOb7tZEjj0g4kMh1spANU3fkmRdbzXUHi-vYAIMjCPZltkzZEs65JvyU-y4E-WoAgRU8_saK5hdMo-NTv3&uniplatform=NZKPT&language=CHS (accessed on 1 April 2023).
62. Zhang, Y.; Lv, X.; Li, S.; Chen, H.; Quan, X.; Zhou, X.; Dong, Z. Preparation and properties of graphene supported NiCoMn LDH catalysts. *J. Shenyang Ligong Univ.* **2022**, *41*, 47–52. Available online: https://kns.cnki.net/kcms2/article/abstract?v=BS8_DD2Uwa4iwj6y0c2gAeym2zLqE79t4l-iwUPVKbidgefKtDwqXKJXG0JftN8yVnopc23ziBQH71c-3U0-d2d1LhG9XVUu4hlwIGiTrvlm1obiAQ5gQIgD3CjrCrr6KZEbsctE_6Hcy9L8K_qkUhtf2Xp7wair&uniplatform=NZKPT&language=CHS (accessed on 1 October 2022).
63. Song, Y.; Ji, K.; Duan, H.; Shao, M. Hydrogen production coupled with water and organic oxidation based on layered double hydroxides. *Exploration* **2021**, *1*, 20210050. [CrossRef] [PubMed]
64. Liu, W.-J.; Dang, L.; Xu, Z.; Yu, H.-Q.; Jin, S.; Huber, G.W. Electrochemical Oxidation of 5-Hydroxymethylfurfural with NiFe Layered Double Hydroxide (LDH) Nanosheet Catalysts. *ACS Catal.* **2018**, *8*, 5533–5541. [CrossRef]
65. Zhang, M.; Liu, Y.; Liu, B.; Chen, Z.; Xu, H.; Yan, K. Trimetallic NiCoFe-Layered Double Hydroxides Nanosheets Efficient for Oxygen Evolution and Highly Selective Oxidation of Biomass-Derived 5-Hydroxymethylfurfural. *ACS Catal.* **2020**, *10*, 5179–5189. [CrossRef]
66. Qi, Y.-F.; Wang, K.-Y.; Sun, Y.; Wang, J.; Wang, C. Engineering the Electronic Structure of NiFe Layered Double Hydroxide Nanosheet Array by Implanting Cationic Vacancies for Efficient Electrochemical Conversion of 5-Hydroxymethylfurfural to 2,5-Furandicarboxylic Acid. *ACS Sustain. Chem. Eng.* **2022**, *10*, 645–654. [CrossRef]
67. Zhong, Y.; Ren, R.-Q.; Wang, J.-B.; Peng, Y.-Y.; Li, Q.; Fan, Y.-M. Grass-like Ni₉Se₇ nanowire arrays shelled with NiFe LDH nanosheets as a 3D hierarchical core-shell electrocatalyst for efficient upgrading of biomass-derived 5-hydroxymethylfurfural and furfural. *Catal. Sci. Technol.* **2022**, *12*, 201–211. [CrossRef]
68. Dhanasmoro, L.; Li, O.L. Highly active NiFe LDH anchoring on cobalt carbonate hydroxide for efficient electrocatalytic 5-hydroxymethylfurfural oxidation towards 2,5-furandicarboxylic acid. *New J. Chem.* **2023**, *47*, 14282–14288. [CrossRef]
69. Liu, B.; Zheng, Z.; Liu, Y.; Zhang, M.; Wang, Y.; Wan, Y.; Yan, K. Efficient electrooxidation of biomass-derived aldehydes over ultrathin NiV-layered double hydroxides films. *J. Energy Chem.* **2023**, *78*, 412–421. [CrossRef]
70. Pang, X.; Bai, H.; Zhao, H.; Fan, W.; Shi, W. Efficient Electrocatalytic Oxidation of 5-Hydroxymethylfurfural Coupled with 4-Nitrophenol Hydrogenation in a Water System. *ACS Catal.* **2022**, *12*, 1545–1557. [CrossRef]
71. Huang, Y.; Pang, X.; Cui, J.; Huang, Z.; Wang, G.; Zhao, H.; Bai, H.; Fan, W. Strengthening the Stability of the Reconstructed NiOOH Phase for 5-Hydroxymethylfurfural Oxidation. *Inorg. Chem.* **2023**, *62*, 6499–6509. [CrossRef]
72. Yang, Z.; Zhang, B.; Yan, C.; Xue, Z.; Mu, T. The pivot to achieve high current density for biomass electrooxidation: Accelerating the reduction of Ni³⁺ to Ni²⁺. *Appl. Catal. B* **2023**, *330*, 122590. [CrossRef]
73. Zhou, Z.; Chen, C.; Gao, M.; Xia, B.; Zhang, J. In situ anchoring of a Co₃O₄ nanowire on nickel foam: An outstanding bifunctional catalyst for energy-saving simultaneous reactions. *Green Chem.* **2019**, *21*, 6699–6706. [CrossRef]
74. Wang, C.; Bongard, H.-J.; Weidenthaler, C.; Wu, Y.; Schüth, F. Design and Application of a High-Surface-Area Mesoporous δ-MnO₂ Electrocatalyst for Biomass Oxidative Valorization. *Chem. Mater.* **2022**, *34*, 3123–3132. [CrossRef]
75. Zhu, B.; Qin, Y.; Du, J.; Zhang, F.; Lei, X. Ammonia Etching to Generate Oxygen Vacancies on CuMn₂O₄ for Highly Efficient Electrocatalytic Oxidation of 5-Hydroxymethylfurfural. *ACS Sustain. Chem. Eng.* **2021**, *9*, 11790–11797. [CrossRef]
76. Lu, Y.; Dong, C.-L.; Huang, Y.-C.; Zou, Y.; Liu, Z.; Liu, Y.; Li, Y.; He, N.; Shi, J.; Wang, S. Identifying the Geometric Site Dependence of Spinel Oxides for the Electrooxidation of 5-Hydroxymethylfurfural. *Angew. Chem. Int. Ed.* **2020**, *59*, 19215–19221. [CrossRef] [PubMed]

77. Wei, T.; Liu, W.; Zhang, S.; Liu, Q.; Luo, J.; Liu, X. A dual-functional Bi-doped Co_3O_4 nanosheet array towards high efficiency 5-hydroxymethylfurfural oxidation and hydrogen production. *Chem. Commun.* **2023**, *59*, 442–445. [[CrossRef](#)] [[PubMed](#)]
78. Zhong, R.; Wang, Q.; Du, L.; Pu, Y.; Ye, S.; Gu, M.; Conrad Zhang, Z.; Huang, L. Ultrathin polycrystalline Co_3O_4 nanosheets with enriched oxygen vacancies for efficient electrochemical oxygen evolution and 5-hydroxymethylfurfural oxidation. *Appl. Surf. Sci.* **2022**, *584*, 152553. [[CrossRef](#)]
79. Sun, M.; Wang, Y.; Sun, C.; Qi, Y.; Cheng, J.; Song, Y.; Zhang, L. Nitrogen-doped Co_3O_4 nanowires enable high-efficiency electrochemical oxidation of 5-hydroxymethylfurfural. *Chin. Chem. Lett.* **2022**, *33*, 385–389. [[CrossRef](#)]
80. Zhong, R.; Wu, P.; Wang, Q.; Zhang, X.; Du, L.; Liu, Y.; Yang, H.; Gu, M.; Zhang, Z.C.; Huang, L.; et al. Room-temperature fabrication of defective CoOxHy nanosheets with abundant oxygen vacancies and high porosity as efficient 5-hydroxymethylfurfural oxidation electrocatalysts. *Green Chem.* **2023**, *25*, 4674–4684. [[CrossRef](#)]
81. Wang, W.; Zhang, Z.; Wang, M. Preparation of NiO-N/C composites for electrochemical oxidation of 5-hydroxymethylfurfural to 2,5-furandicarboxylic acid. *Biomass Convers. Biorefin.* **2022**, *13*, 17247–17254. [[CrossRef](#)]
82. Guo, Z.-Y.; Li, C.-X.; Gao, M.; Han, X.; Zhang, Y.-J.; Zhang, W.-J.; Li, W.-W. Mn-O Covalency Governs the Intrinsic Activity of Co-Mn Spinel Oxides for Boosted Peroxymonosulfate Activation. *Angew. Chem. Int. Ed.* **2021**, *60*, 274–280. [[CrossRef](#)]
83. Yang, G.; Jiao, Y.; Yan, H.; Xie, Y.; Wu, A.; Dong, X.; Guo, D.; Tian, C.; Fu, H. Interfacial Engineering of MoO_2 -FeP Heterojunction for Highly Efficient Hydrogen Evolution Coupled with Biomass Electrooxidation. *Adv. Mater.* **2020**, *32*, 2000455. [[CrossRef](#)]
84. Lu, Y.; Dong, C.-L.; Huang, Y.-C.; Zou, Y.; Liu, Y.; Li, Y.; Zhang, N.; Chen, W.; Zhou, L.; Lin, H.; et al. Hierarchically nanostructured NiO- Co_3O_4 with rich interface defects for the electro-oxidation of 5-hydroxymethylfurfural. *Sci. China Chem.* **2020**, *63*, 980–986. [[CrossRef](#)]
85. Gao, L.; Liu, Z.; Ma, J.; Zhong, L.; Song, Z.; Xu, J.; Gan, S.; Han, D.; Niu, L. NiSe@NiOx core-shell nanowires as a non-precious electrocatalyst for upgrading 5-hydroxymethylfurfural into 2,5-furandicarboxylic acid. *Appl. Catal. B* **2020**, *261*, 118235. [[CrossRef](#)]
86. Liang, S.; Pan, L.; Thomas, T.; Zhu, B.; Chen, C.; Zhang, J.; Shen, H.; Liu, J.; Yang, M. $\text{Ni}_3\text{N-V}_2\text{O}_3$ enables highly efficient 5-(Hydroxymethyl) furfural oxidation enabling membrane free hydrogen production. *Chem. Eng. J.* **2021**, *415*, 128864. [[CrossRef](#)]
87. Wang, H.; Zhou, Y.; Tao, S. CoP-CoOOH heterojunction with modulating interfacial electronic structure: A robust biomass-upgrading electrocatalyst. *Appl. Catal. B* **2022**, *315*, 121588. [[CrossRef](#)]
88. Chen, J.; Wang, Y.; Zhou, M.; Li, Y. Boosting the electro-oxidation of 5-hydroxymethyl-furfural on a Co-CoSx heterojunction by intensified spin polarization. *Chem. Sci.* **2022**, *13*, 4647–4653. [[CrossRef](#)] [[PubMed](#)]
89. Zhou, M.; Chen, J.; Li, Y. CoP nanorods anchored on $\text{Ni}_2\text{P-NiCoP}$ nanosheets with abundant heterogeneous interfaces boosting the electrocatalytic oxidation of 5-hydroxymethyl-furfural. *Catal. Sci. Technol.* **2022**, *12*, 4288–4297. [[CrossRef](#)]
90. Luo, R.; Li, Y.; Xing, L.; Wang, N.; Zhong, R.; Qian, Z.; Du, C.; Yin, G.; Wang, Y.; Du, L. A dynamic Ni(OH)_2 -NiOOH/NiFeP heterojunction enabling high-performance E-upgrading of hydroxymethylfurfural. *Appl. Catal. B* **2022**, *311*, 121357. [[CrossRef](#)]
91. Zeng, J.; Chen, W.; Zhang, G.; Yu, L.; Zhong, L.; Liu, Y.; Zhao, S.; Qiu, Y. Heterostructured $\text{Ni}_3\text{N-NiMoN}$ Nanowires as Bifunctional Electrocatalysts for Hydrogen Evolution and 5-Hydroxymethylfurfural Oxidation. *ACS Appl. Nano Mater.* **2022**, *5*, 7321–7330. [[CrossRef](#)]
92. Xu, D.; Yang, Y.; Zhang, B.; Yang, Z.; Liu, S.; Mu, T. Deep Eutectic Solvent-Induced In Situ Etching and Phosphorization to Form Nickel Phosphides for Electrooxidation of 5-Hydroxymethylfurfural. *ChemSusChem* **2022**, *15*, e202200822. [[CrossRef](#)] [[PubMed](#)]
93. Xing, M.; Zhang, D.; Liu, D.; Song, C.; Wang, D. Surface engineering of carbon-coated cobalt-doped nickel phosphides bifunctional electrocatalyst for boosting 5-hydroxymethylfurfural oxidation coupled with hydrogen evolution. *J. Colloid Interface Sci.* **2023**, *629*, 451–460. [[CrossRef](#)] [[PubMed](#)]
94. Zhao, G.; Hai, G.; Zhou, P.; Liu, Z.; Zhang, Y.; Peng, B.; Xia, W.; Huang, X.; Wang, G. Electrochemical Oxidation of 5-Hydroxymethylfurfural on CeO_2 -Modified Co_3O_4 with Regulated Intermediate Adsorption and Promoted Charge Transfer. *Adv. Funct. Mater.* **2023**, *33*, 2213170. [[CrossRef](#)]
95. Zhou, P.; Hai, G.; Zhao, G.; Li, R.; Huang, X.; Lu, Y.; Wang, G. CeO_2 as an “electron pump” to boost the performance of Co_4N in electrocatalytic hydrogen evolution, oxygen evolution and biomass oxidation valorization. *Appl. Catal. B* **2023**, *325*, 122364. [[CrossRef](#)]
96. Bi, J.; Xu, H.; Wang, W.; Sang, T.; Jiang, A.; Hao, J.; Li, Z. Cu_2P_7 -CoP Heterostructure Nanosheets Enable High-Performance of 5-Hydroxymethylfurfural Electrooxidation. *Chemistry* **2023**, *29*, e202300973. [[CrossRef](#)]
97. Zhang, B.; Fu, H.; Mu, T. Hierarchical $\text{NiSx/Ni}_2\text{P}$ nanotube arrays with abundant interfaces for efficient electrocatalytic oxidation of 5-hydroxymethylfurfural. *Green Chem.* **2022**, *24*, 877–884. [[CrossRef](#)]
98. Luo, R.; Li, Y.; Wang, N.; Zhong, R.; Xing, L.; Zhu, L.; Wang, Y.; Du, L.; Ye, S. A Bimetallic Phosphide@Hydroxide Interface for High-Performance 5-Hydroxymethylfurfural Electro-Valorization. *J. Phys. Chem. C* **2023**, *127*, 4967–4974. [[CrossRef](#)]
99. Li, Y.; Fu, Y.; Cao, Y.; Lei, F.; Zhao, J.; Wang, R.; Qiu, S.; Zhang, Z. Construction of hierarchical NiCu-based bimetallic electrocatalysts for promoting the electrooxidation of biomass derivatives. *Sustain. Energy Fuels* **2023**, *7*, 4505–4513. [[CrossRef](#)]
100. Sun, M.; Yang, J.; Huang, J.; Wang, Y.; Liu, X.; Qi, Y.; Zhang, L. Interfacial Engineering of Ni/ $\text{Ni}_{0.2}\text{Mo}_{0.8}\text{N}$ Heterostructured Nanorods Realizes Efficient 5-Hydroxymethylfurfural Electrooxidation and Hydrogen Evolution. *Langmuir* **2023**, *39*, 3762–3769. [[CrossRef](#)]
101. Jia, W.; Liu, B.; Gong, R.; Bian, X.; Du, S.; Ma, S.; Song, Z.; Ren, Z.; Chen, Z. Electronic Modulation Induced by Ni-VN Heterojunction Reinforces Electrolytic Hydrogen Evolution Coupled with Biomass Upgrade. *Small* **2023**, *19*, 2302025. [[CrossRef](#)]

102. Wu, J.; Chen, J.; Yu, T.; Zhai, Z.; Zhu, Y.; Wu, X.; Yin, S. Boosting Electrochemical Kinetics of NiCo₂ via MoO₂ Modification for Biomass Upgrading Assisted Hydrogen Evolution. *ACS Catal.* **2023**, *13*, 13257–13266. [[CrossRef](#)]
103. Woo, J.; Moon, B.C.; Lee, U.; Oh, H.-S.; Chae, K.H.; Jun, Y.; Min, B.K.; Lee, D.K. Collaborative Electrochemical Oxidation of the Alcohol and Aldehyde Groups of 5-Hydroxymethylfurfural by NiOOH and Cu(OH)₂ for Superior 2,5-Furandicarboxylic Acid Production. *ACS Catal.* **2022**, *12*, 4078–4091. [[CrossRef](#)]
104. Xue, Y.; Zhao, G.; Yang, R.; Chu, F.; Chen, J.; Wang, L.; Huang, X. 2D metal–organic framework-based materials for electrocatalytic, photocatalytic and thermocatalytic applications. *Nanoscale* **2021**, *13*, 3911–3936. [[CrossRef](#)] [[PubMed](#)]
105. Zhou, P.; Lv, J.; Huang, X.; Lu, Y.; Wang, G. Strategies for enhancing the catalytic activity and electronic conductivity of MOFs-based electrocatalysts. *Coord. Chem. Rev.* **2023**, *478*, 214969. [[CrossRef](#)]
106. Phan, D.-P.; Tran, M.H.; Lee, E.Y. Metal-organic framework-based materials as heterogeneous catalysts for biomass upgrading into renewable plastic precursors. *Mater. Today Chem.* **2023**, *33*, 101691. [[CrossRef](#)]
107. Li, Y.; Wu, Y.; Liu, K.; Delbari, S.A.; Kim, A.; Sabahi Namini, A.; Le, Q.V.; Shokouhimehr, M.; Xia, C.; Jang, H.W.; et al. Metal-organic framework-based nanostructured catalysts: Applications in biomass conversion. *Fuel* **2023**, *340*, 127482. [[CrossRef](#)]
108. Cai, M.; Zhang, Y.; Zhao, Y.; Liu, Q.; Li, Y.; Li, G. Two-dimensional metal–organic framework nanosheets for highly efficient electrocatalytic biomass 5-(hydroxymethyl)furfural (HMF) valorization. *J. Mater. Chem. A* **2020**, *8*, 20386–20392. [[CrossRef](#)]
109. Pila, T.; Nueangnoraj, K.; Ketrat, S.; Somjit, V.; Kongpatpanich, K. Electrochemical Production of 2,5-Furandicarboxylic from 5-Hydroxymethylfurfural Using Ultrathin Co(OH)₂ on ZIF-67. *ACS Appl. Energy Mater.* **2021**, *4*, 12909–12916. [[CrossRef](#)]
110. Bai, X.-J.; He, W.-X.; Lu, X.-Y.; Fu, Y.; Qi, W. Electrochemical oxidation of 5-hydroxymethylfurfural on ternary metal–organic framework nanoarrays: Enhancement from electronic structure modulation. *J. Mater. Chem. A* **2021**, *9*, 14270–14275. [[CrossRef](#)]
111. Sekar, P.; Vasanthakumar, P.; Shanmugam, R.; Senthil Kumar, S.; Agnoli, S.; Deepak, R.J.; Murugan, K.; Bhuvanesh, N.; Karvembu, R. Green synthesis of a redox-active riboflavin-integrated Ni-MOF and its versatile electrocatalytic applications towards oxygen evolution and reduction, and HMF oxidation reactions. *Green Chem.* **2022**, *24*, 9233–9244. [[CrossRef](#)]
112. Zhang, Y.; Kornienko, N. Conductive Metal-Organic Frameworks Bearing M–O₄ Active Sites as Highly Active Biomass Valorization Electrocatalysts. *ChemSusChem* **2022**, *15*, e202101587. [[CrossRef](#)]
113. Pang, X.; Zhao, H.; Huang, Y.; Luo, B.; Bai, H.; Fan, W. Electrochemically induced NiOOH/Ag⁺ active species for efficient oxidation of 5-hydroxymethylfurfural. *Appl. Surf. Sci.* **2023**, *608*, 155152. [[CrossRef](#)]
114. Pang, X.; Bai, H.; Huang, Y.; Zhao, H.; Zheng, G.; Fan, W. Mechanistic insights for dual-species evolution toward 5-hydroxymethylfurfural oxidation. *J. Catal.* **2023**, *417*, 22–34. [[CrossRef](#)]
115. Feng, Y.; Yang, K.; Smith, R.L.; Qi, X. Metal sulfide enhanced metal–organic framework nanoarrays for electrocatalytic oxidation of 5-hydroxymethylfurfural to 2,5-furandicarboxylic acid. *J. Mater. Chem. A* **2023**, *11*, 6375–6383. [[CrossRef](#)]
116. Cai, M.; Ding, S.; Gibbons, B.; Yang, X.; Kessinger, M.C.; Morris, A.J. Nickel(ii)-modified covalent-organic framework film for electrocatalytic oxidation of 5-hydroxymethylfurfural (HMF). *Chem. Commun.* **2020**, *56*, 14361–14364. [[CrossRef](#)]
117. Qin, Q.; Heil, T.; Schmidt, J.; Schmallegger, M.; Gescheidt, G.; Antonietti, M.; Oschatz, M. Electrochemical Fixation of Nitrogen and Its Coupling with Biomass Valorization with a Strongly Adsorbing and Defect Optimized Boron–Carbon–Nitrogen Catalyst. *ACS Appl. Energy Mater.* **2019**, *2*, 8359–8365. [[CrossRef](#)]
118. Ma, T.; Kapustin, E.A.; Yin, S.X.; Liang, L.; Zhou, Z.; Niu, J.; Li, L.-H.; Wang, Y.; Su, J.; Li, J.; et al. Single-crystal X-ray diffraction structures of covalent organic frameworks. *Science* **2018**, *361*, 48–52. [[CrossRef](#)] [[PubMed](#)]
119. Yang, L.; Shao, L.; Wu, Z.; Zhan, P.; Zhang, L. Design and Synthesis of Porous Organic Polymers: Promising Catalysts for Lignocellulose Conversion to 5-Hydroxymethylfurfural and Derivates. *Polymers* **2023**, *15*, 2630. [[CrossRef](#)]

Disclaimer/Publisher’s Note: The statements, opinions and data contained in all publications are solely those of the individual author(s) and contributor(s) and not of MDPI and/or the editor(s). MDPI and/or the editor(s) disclaim responsibility for any injury to people or property resulting from any ideas, methods, instructions or products referred to in the content.